Calhoun: The NPS Institutional Archive

DSpace Repository

Theses and Dissertations | 1. Thesis and Dissertation Collection, all items

2010

Modeling of the electric ship

Pifer, Ryan James

Monterey, California. Naval Postgraduate School

http://hdl.handle.net/10945/5254

This publication is a work of the U.S. Government as defined in Title 17, United States Code, Section 101. Copyright protection is not available for this work in the United States.

Downloaded from NPS Archive: Calhoun

http://www.nps.edu/library

Calhoun is the Naval Postgraduate School's public access digital repository for research materials and institutional publications created by the NPS community. Calhoun is named for Professor of Mathematics Guy K. Calhoun, NPS's first appointed -- and published -- scholarly author.

Dudley Knox Library / Naval Postgraduate School
411 Dyer Road / 1 University Circle
Monterey, California USA 93943

NAVAL POSTGRADUATE SCHOOL

MONTEREY, CALIFORNIA

THESIS

MODELING OF THE ELECTRIC SHIP

by

Ryan James Pifer

June 2010

Thesis Advisor: William Colson
Thesis Co-Advisor: Keith Cohn

Approved for public release; distribution is unlimited

THIS PAGE INTENTIONALLY LEFT BLANK

REPORT DOCUMENTATION PAGE		*Form Approved OMB No. 0704-0188*
Public reporting burden for this collection of information is estimated to average 1 hour per response, including the time for reviewing instruction, searching existing data sources, gathering and maintaining the data needed, and completing and reviewing the collection of information. Send comments regarding this burden estimate or any other aspect of this collection of information, including suggestions for reducing this burden, to Washington headquarters Services, Directorate for Information Operations and Reports, 1215 Jefferson Davis Highway, Suite 1204, Arlington, VA 22202-4302, and to the Office of Management and Budget, Paperwork Reduction Project (0704-0188) Washington DC 20503.		
1. AGENCY USE ONLY *(Leave blank)*	**2. REPORT DATE** June 2010	**3. REPORT TYPE AND DATES COVERED** Master's Thesis
4. TITLE AND SUBTITLE Modeling of the Electric Ship		**5. FUNDING NUMBERS**
6. AUTHOR(S) Ryan Pifer		
7. PERFORMING ORGANIZATION NAME(S) AND ADDRESS(ES) Naval Postgraduate School Monterey, CA 93943-5000		**8. PERFORMING ORGANIZATION REPORT NUMBER**
9. SPONSORING /MONITORING AGENCY NAME(S) AND ADDRESS(ES) N/A		**10. SPONSORING/MONITORING AGENCY REPORT NUMBER**
11. SUPPLEMENTARY NOTES The views expressed in this thesis are those of the author and do not reflect the official policy or position of the Department of Defense or the U.S. Government. IRB Protocol number _____.		
12a. DISTRIBUTION / AVAILABILITY STATEMENT Approved for public release; distribution is unlimited		**12b. DISTRIBUTION CODE**

13. ABSTRACT (maximum 200 words)

As the United States Navy continues to refine its designs for future ships, one approach that it is currently being explored is to use a unified electrical grid to power every system aboard a ship, including propulsion and weapons. Some concerns with this design are estimating the power demands placed upon the grid by various systems and anticipating transients induced on the grid by high power pulsed loads.

The first part of this thesis will focus on the free electron laser (FEL). The FEL will require a substantial amount of power during an engagement; even at reduced levels of readiness, the FEL will still need residual amounts of power in order to fire the weapon in a reasonable amount of time. This thesis will present the power estimates of the FEL for five states of readiness, and will discuss the results of a computer model developed in collaboration with the University of Texas at Austin.

The second part of this thesis will focus on the electromagnetic railgun. Specifically, I have developed a model that simulates the charging and discharging an energy storage capacitor and will present the results.

14. SUBJECT TERMS Free Electron Laser, Railgun, Electric Ship, Laser Weapons System, Integrated Power System			**15. NUMBER OF PAGES** 95
			16. PRICE CODE
17. SECURITY CLASSIFICATION OF REPORT Unclassified	**18. SECURITY CLASSIFICATION OF THIS PAGE** Unclassified	**19. SECURITY CLASSIFICATION OF ABSTRACT** Unclassified	**20. LIMITATION OF ABSTRACT** UU

NSN 7540-01-280-5500 Standard Form 298 (Rev. 2-89)
Prescribed by ANSI Std. 239-18

THIS PAGE INTENTIONALLY LEFT BLANK

Approved for public release; distribution is unlimited

MODELING OF THE ELECTRIC SHIP

Ryan James Pifer
Ensign, United States Navy
United States Naval Academy, 2009

Submitted in partial fulfillment of the
requirements for the degree of

MASTER OF SCIENCE IN PHYSICS

from the

NAVAL POSTGRADUATE SCHOOL
June 2010

Author: Ryan Pifer

Approved by: William B. Colson
Thesis Advisor

Keith Cohn
Co-Advisor

Robert Armstead
Second Reader

Andres Larraza
Chairman, Department of Physics

THIS PAGE INTENTIONALLY LEFT BLANK

ABSTRACT

As the United States Navy continues to refine its designs for future ships, one approach that it is currently being explored is to use a unified electrical grid to power every system aboard a ship, including propulsion and weapons. Some concerns with this design are estimating the power demands placed upon the grid by various systems and anticipating transients induced on the grid by high power pulsed loads.

The first part of this thesis will focus on the free electron laser (FEL). The FEL will require a substantial amount of power during an engagement; even at reduced levels of readiness, the FEL will still need residual amounts of power in order to fire the weapon in a reasonable amount of time. This thesis will present the power estimates of the FEL for five states of readiness, and will discuss the results of a computer model developed in collaboration with the University of Texas at Austin.

The second part of this thesis will focus on the electromagnetic railgun. Specifically I have developed of a model that simulates the charging and discharging an energy storage capacitor and will present the results.

THIS PAGE INTENTIONALLY LEFT BLANK

TABLE OF CONTENTS

I. INTRODUCTION 1

II. ELECTRIC SHIP BACKGROUND 3

A. SEGREGATED POWER SYSTEMS 3

B. INTEGRATED POWER SYSTEMS 4

1. Power 5

2. Benefits 6

3. Looking Forward 7

III. ELECTRIC MOTORS 9

A. DC MOTORS 9

1. DC Homopolar Motors 10

2. DC Superconducting Homopolar Motors 11

B. AC MOTORS 12

1. AC Synchronous Motors 13

2. High Temperature Superconducting AC Synchronous Motors 13

3. AC Induction Motors 14

IV. THE FREE ELECTRON LASER 17

V. THE FREE ELECTRON LASER MODEL 23

A. SYSTEM DESCRIPTIONS 24

1. Cryogenics System 24

2. Cathode 25

3. Injector and Linac 25

4. Beam Dump 26

5. Other Loads 26

B. STATES OF READINESS 27

1. Pier Side 28

2. Underway 30
3. Hot Standby 31
4. Engagement 32
5. Operational Readiness, Between Shots 33
C. RESULTS 34
1. Control Run 35
2. Pier Side to Underway 39
3. Underway to Hot Standby 41
4. Hot Standby to Engagement 43
5. Engagement to Operational Readiness Between Shots 45
VI. THE RAILGUN 47
VII. THE RAILGUN MODEL 51
A. POWER SUPPLY AND ENERGY STORAGE 51
1. The Model 53
B. RAILS AND PROJECTILE 56
1. The Model 57
2. Rail Inductance 58
3. Rail Resistance 59
4. Force on the Projectile 60
C. RESULTS 60
1. Charging Results 60
2. Firing Results 62
VIII. THE LASER WEAPONS SYSTEM 67
IX. CONCLUSION 71
LIST OF REFERENCES 73
INITIAL DISTRIBUTION LIST 75

LIST OF FIGURES

1. Comparison Between a Segregated Power System and an Integrated Power System 4
2. Projected Current Advancement Path for the Integrated Power System 6
3. Weight Distribution Model Comparison for a Traditionally-Powered Ship and a Ship Using an Integrated Power System 8
4. Simple Solenoid 9
5. Simple DC Motor Design 10
6. Simple DC Homopolar Motor Design 11
7. DC Superconducting Homopolar Motor by General Atomics 12
8. Simple AC Motor Design 13
9. High Temperature Superconducting AC Synchronous Motor by American Superconductor 14
10. Simple AC Induction Motor Design 15
11. AC Induction Motor by Converteam 16
12. Electron Energy Transitions 17
13. Basic Free Electron Laser Design 18
14. Phallanx Close-In Weapons System 21
15. Simulink Model of FEL Simulation on an Electric Ship 23
16. FEL Model Components 24
17. FEL Components at Pier Side State of Readiness 29
18. FEL Components at Underway State of Readiness 30
19. FEL Components at Hot Standby State of Readiness 31
20. FEL Components at Engagement State of Readiness 32
21. FEL Components at Operational Readiness Between Shots State of Readiness 33
22. 6000VDC Bus Voltage Output, Control Run 36

23. 4160VAC Bus RMS Voltage Output, Control Run 36
24. 450VAC Bus Voltage Output, Control Run 37
25. 113VAC Bus Voltage Output, Control Run 37
26. 45kVDC Bus Voltage Output, Control Run 38
27. 800VDC Bus Voltage Output, Control Run 38
28. 6000VDC Bus Voltage Output, Pier Side to Underway 39
29. 4160VAC Bus RMS Voltage Output, Pier Side to Underway 40
30. 450VAC Bus Voltage Output, Pier Side to Underway 40
31. 450VAC Bus Voltage Output, Underway to Hot Standby 41
32. 45kVDC Bus Voltage Output, Underway to Hot Standby 42
33. 800VDC Bus Voltage Output, Underway to Hot Standby 42
34. 800VDC Bus Voltage Output-Enlarged, Underway to Hot Standby . . 43
35. 45kVDC Bus Current Output, Hot Standby to Engagement 44
36. 45kVDC Bus Current Output-Enlarged, Hot Standby to Engagement . 44
37. Simple Railgun Design 48
38. Buck-Boost Converter 51
39. Buck-Boost Converter, Switch Closed and Open 52
40. Buck-Boost Converter, Switch Closed 54
41. Buck-Boost Converter, Switch Open 55
42. Labeled Rail Dimensions 56
43. Railgun Circuit-Loop 58
44. Capacitor Charge, Charging Phase, Five Shots 61
45. Peak Circuit Current, Charging Phase, Five Shots 61
46. Velocity of Projectile in Barrel During Firing, One Shot 63
47. Acceleration of Projectile in Barrel During Firing, One Shot 64
48. Inductance of Rails During Firing, One Shot 64
49. Resistance of Rails During Firing, One Shot 65
50. Current in Rails During Firing, One Shot 65

51. Laser Weapons System Integrated Onto Close-In Weapon System . . . 67
52. Fiber Optic Laser Merging for Laser Weapons System 68
53. Laser Weapons System Prototype 69

THIS PAGE INTENTIONALLY LEFT BLANK

LIST OF TABLES

I. FEL Model States of Readiness 28
II. Index of Railgun Component Specifications and Symbols for the Charging Portion 53
III. Index of Railgun Component Specifications and Symbols for the Firing Portion 57

THIS PAGE INTENTIONALLY LEFT BLANK

LIST OF ACRONYMS AND ABBREVIATIONS

Symbol	Description
A	Ampere
AC	Alternating Current
ACSM	AC Synchronous Motor
C	Coulomb
CEM	Center for Electromechanics
CIWS	Close-In Weapon System
DC	Direct Current
ERL	Energy Recovery Linear Accelerator
F	Farad
FEL	Free Electron Laser
Gs	Earth Gravitational Units
H	Henry
HTS	High Temperature Superconducting
Hz	Hertz
IPS	Integrated Power System
J	Joule
K	Kelvin
kA	Kiloamps
kg	Kilogram
km	Kilometer
km/s	Kilometers per Second
kVAC	Kilovolts Alternating Current
kVDC	Kilovolts Direct Current
kW	Kilowatt
LaWS	Laser Weapons System
Linac	Linear Accelerator
m	Meter
m/s	Meters per Second
MeV	Mega-Electron-Volt
MJ	Megajoule
mm	Millimeter
ms	Millisecond
MVAC	Medium Voltage AC
NPS	Naval Postgraduate School
MVDC	Medium Voltage DC

MW	Megawatt
NAVSEA	Naval Sea Systems Command
nm	Nanometer
ns	Nanosecond
RF	Radio Frequency
RMS	Root Mean Squared
s	Second
SDCHM	Superconducting DC Homopolar Motor
UAV	Unmanned Aerial Vehicle
UTA	University of Texas at Austin
VAC	Volts AC
VDC	Volts DC
μF	Microfarad
μs	Microsecond
$\mu\Omega$	Microohm
Ω	Ohm

ACKNOWLEDGMENTS

I would like to first thank the United States Navy for giving me the opportunity to earn a bachelor's degree at the Naval Academy and then immediately work towards a master's degree here at the Naval Postgraduate School.

Secondly, I want to extend a thanks to all who helped me in this process: Professors Bill Colson, Keith Cohn, and Bob Armstead, at the Naval Postgraduate School, and Dr. Angelo Gattozzi and Professor Robert Hebner, at the University of Texas at Austin.

Finally, I would like to thank my family: my parents, Valerie and James, and my sisters, Lindsey and Hannah, for their support over the years.

THIS PAGE INTENTIONALLY LEFT BLANK

I. INTRODUCTION

Technology aboard ships and submarines has dramatically improved in the last half century. With that improvement comes the need for more energy to power the advanced systems that have been developed. Increasing the amount of power available to non-propulsion systems on traditional ships with segregated systems has reached a wall. While there are proposed ways to temporarily increase the amount of available electricity on existing ship classes, such as the hybrid-electric drive system proposed for the Flight III *Arleigh-Burke*-class destroyer, a more significant change may be needed to provide enough power for future weapons and defensive systems.

That change will likely come as the Integrated Power System (IPS) that is proposed for all future electric ships and submarines, such as the DDG-1000 *Zumwalt*-class destroyer. This thesis will discuss the future electric ship power systems for the U.S. Navy and the various elements that are intended to be included on IPS designs.

Chapter II describes the history of the electric ships, the differences between segregated and integrated power systems, and the benefits that IPS designs provide to electric ships, and what kind of power they will use in future phases.

The elimination of segregated power systems also eliminates conventionally powered propulsion. Chapter III describes the consequences of having to use electric motors instead of reduction gears to power ship propulsion. It also compares the advantages and disadvantages to using DC or AC powered electric motors.

Chapter IV describes the background for one of the weapons system proposed for placement aboard an electric ship, the free electron laser (FEL).

Chapter V then describes in detail the computational model that has been developed for a notional free electron laser and discusses its five operational states of readiness. Then, the results from the model runs are presented.

Chapter VI describes the background for the second weapon system to be explored, the electromagnetic gun, or as it is more commonly referred to, the railgun.

Chapter VII then describes in detail the model that has been developed for a notional railgun and its accompanying energy storage device, and presents the results from this model.

Chapter VIII briefly discusses the laser weapons system (LaWS), a device that is in its prototype stage of development but may be closer to deployment on ships than the FEL. Information for this weapon is in the process of being gathered in order to develop a model in the future, similar to those for the FEL and railgun.

II. ELECTRIC SHIP BACKGROUND

Although it sounds futuristic, an electric ship is not new conceptually nor in practice. In fact, many ships over the years have used an electric drive system. As far back as the commissioning of the *USS Langley* in 1913, the United States' first aircraft carrier, Navy ships have employed turbo-electric drives. Yet, save for a few other ship classes since then, the majority of U.S. Navy ships in the last century have been powered by geared turbines [1]. These segregated systems utilize generators that are specifically designated for either propulsion or ship power but not both. However, in recent years, because of advances in electric generator and electric motor technology, there has been a shift back to considering electric drive systems. The new model that the Navy has been developing is the Integrated Power System (IPS), which will provide many benefits over a segregated system. Developed between 1997 and 2002, the IPS is the design that will be employed, or is already employed, on the DDG-1000 *Zumwalt*-class destroyer, the T-AKE-1 *Lewis-and-Clark*-class cargo ship, the currently suspended CG(X) next generation cruiser, the LHA-6 *Makin-Island*-class amphibious assault ship, the Flight III *Virginia*-class attack submarine, and the CVN-21 *Gerald-Ford*-class aircraft carrier [2], [3].

A. SEGREGATED POWER SYSTEMS

The segregated power system that the Navy employs today was initially favored because it proved more efficient than an electric drive system. The improvement in efficiency occurred when geared turbines were significantly improved, reducing weight and size, thus allowing ships to achieve higher speeds and greater ranges than with a turbo-electric system [4]. In a segregated system, shown in Figure 1, one set of four geared turbines use reduction gears to convert mechanical power into torque that turns the propeller shafts. The spinning shafts then transfer the torque through the hull via bearings that seal against water. Since the propellers are directionally fixed,

the ship must use rudders to change the water flow direction behind the ship in order to steer [1]. The other electric power source contains less powerful turbines (usually about three) and independently powers the rest of the ships electrical needs [4]. The problem with a segregated system is that most of the power normally produced on a modern ship, around 80-100 megawatts (MW), is only available to propulsion since its turbines are isolated. So if higher power is needed for, say, weapon or radar systems, it cannot be siphoned from the propulsion turbines even if propulsion is not being used [1].

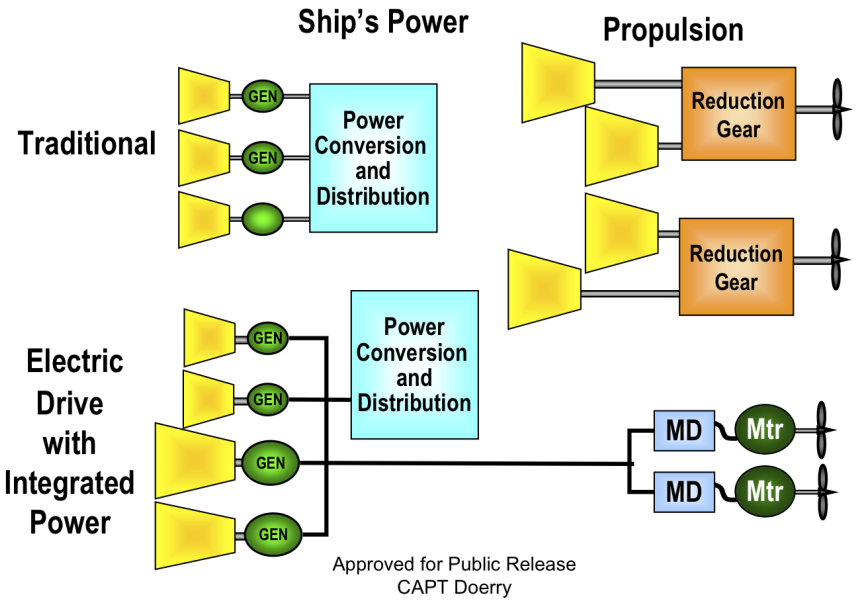

Figure 1. Comparison Between a Segregated Power System and an Integrated Power System. From [2]

B. INTEGRATED POWER SYSTEMS

Integrated power systems, however, are designed to skirt the problem of unavailable power from which segregated power systems suffer. An IPS, pictured in Figure 1, uses fewer prime movers than a segregated system, typically around four.

These prime movers are networked to the ships power grid by a distribution of busses and switches that ensure that vital systems receive appropriate levels of power during casualty scenarios [1]. The prime movers themselves are turbo-electric drives, which use mechanical energy supplied from steam or diesel to power electric generators. The power grid then supplies electricity to the systems that need it. For propulsion, electric motors then convert the electricity back to mechanical power to turn the propellers.

1. Power

The IPS system just described uses turbines that create alternating current (AC) power, converts some of it to direct current (DC) power, and then to the various AC and DC voltage busses. The use of IPS is currently slated to take place in three phases, as seen in Figure 2. The first phase of IPS will use medium voltage AC (MVAC), between 4 and 13.8 kilovolts AC (kVAC) at frequency 60 Hertz (Hz), as implemented in the DDG-1000 and the T-AKE-1 that houses an FM/MAN B&W diesel generator. These systems are meant for ships below 25,000 long tons, which need a high power density, only at 60Hz in operation [2]. The second phase will be high frequency AC that uses the existing AC design, rated between 4 to 13.8kVAC, but that can operate between 60 and 400 Hz. This will likely be used on future small- to medium-sized surface combatants and submarines [2]. The final phase is medium voltage DC rated at 6kVDC, which directly produces the DC power without having to convert AC power.

While the final phase of a 6kVDC power network is the final goal, it is currently not practiced for two reasons. The first is that protective devices for DC power at 6kVDC for MW power ratings do not currently exist. The second is that reliability is still unknown for controllable solid-state switches with voltages greater than 1700 Volts (V) and currents in the kilo-amp (kA) range. The first step to high frequency AC is the most advantageous. The protective devices for existing 60Hz power can be modified for higher frequencies and special electric switches are not needed. In

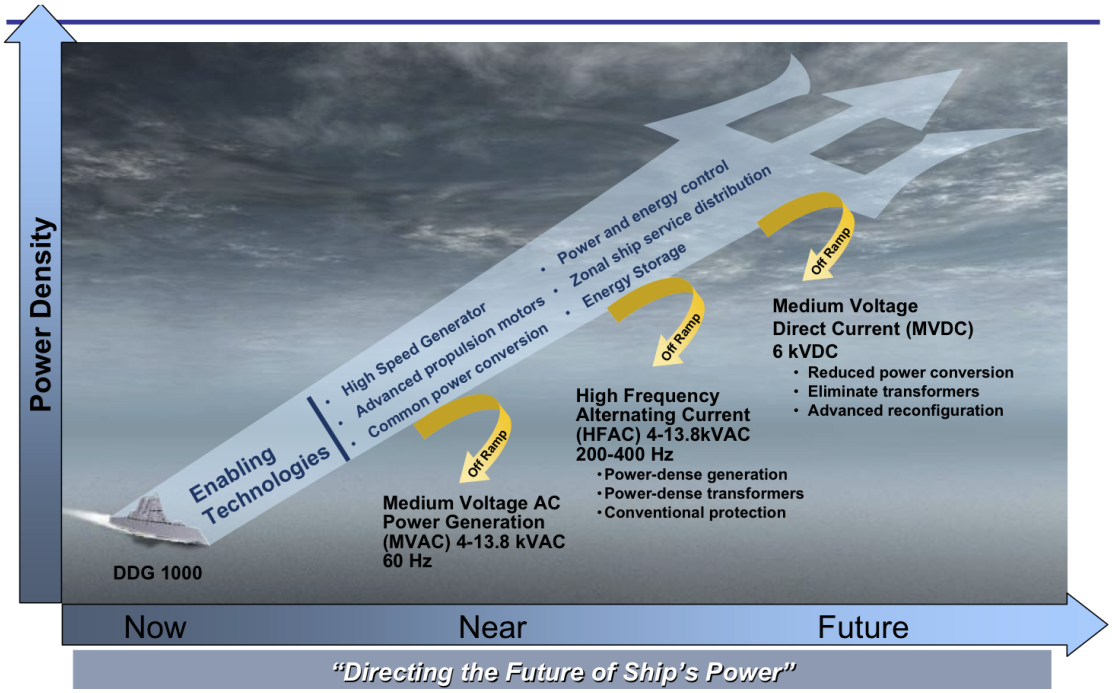

Figure 2. Projected Current Advancement Path for the Integrated Power System. From [2]

addition, the move to higher frequencies will lead to reduction in size of motors, generators and transformers; this is a huge advantage for electric ships [5].

2. Benefits

Shifting from a segregated power system to an IPS has many benefits. First, since the IPS combines all the power generated onto one system, it creates a power-rich environment to supply components demanding high power. This opens up the ship to housing more advanced radars, sonars, and weapons that weren't previously usable since propulsion isolated most of the energy produced for just itself.

Second, the reduced weight from fewer prime movers decreases fuel consumption, as does the greater fuel efficiency of turbo-electric generators. The IPS should also require less maintenance and manpower, cutting additional costs. With all these factors, fuel reduction aboard the future DDG-1000 is estimated at roughly 25%,

saving about $80 million over the life cycle of the ship [1].

Third, the use of an IPS allows for greater freedom in ship design. Since electric ships utilize electric motors that convert DC power back to AC power at the propellers location, a shaft does not need to carry the mechanical energy from the main reduction gear at the turbine site to the propeller. This allows for the turbines and shafts, which are normally in line with the propeller, to be placed in more strategic locations, seen in Figure 3. This also allows the shaft length to be greatly decreased or to be removed altogether in some designs [1]. With this new freedom, ship designers can now redistribute the weight along the keel in ways that can lead to interesting designs in both ships and submarines, such as the DDG-1000 or the next generation fast-attack submarine.

3. Looking Forward

An IPS aboard ships presents opportunities for future developments in seagoing technology. As mentioned, a key advantage to an IPS versus a segregated power system is that the extra power normally reserved for propulsion is now available to the rest of the ship. A complication to this design is the planning required to best distribute the power among the propulsion, weapons and defensive systems under battle conditions. If these high-energy weapons and radars are to be used during full-speed propulsion situations, an energy storage method will be essential as well. Models must also be developed in order to predict how systems will operate during a variety of scenarios and how power usage will affect systems on the ship.

Finally, IPS will provide the opportunity to change shaft, reduction gear and turbine placements from current segregated power locations to more ideal locations via new methods of propulsion. One case being investigated uses a short shaft placed inside the hull directly where the propeller is, and immediately connects to an electric motor. The second case, which is already used by cruise liners and cargo ships, will greatly change the way naval ships are accelerated through the water. This case employs “pods” outside the ship, containing the propeller and an electric motor. These

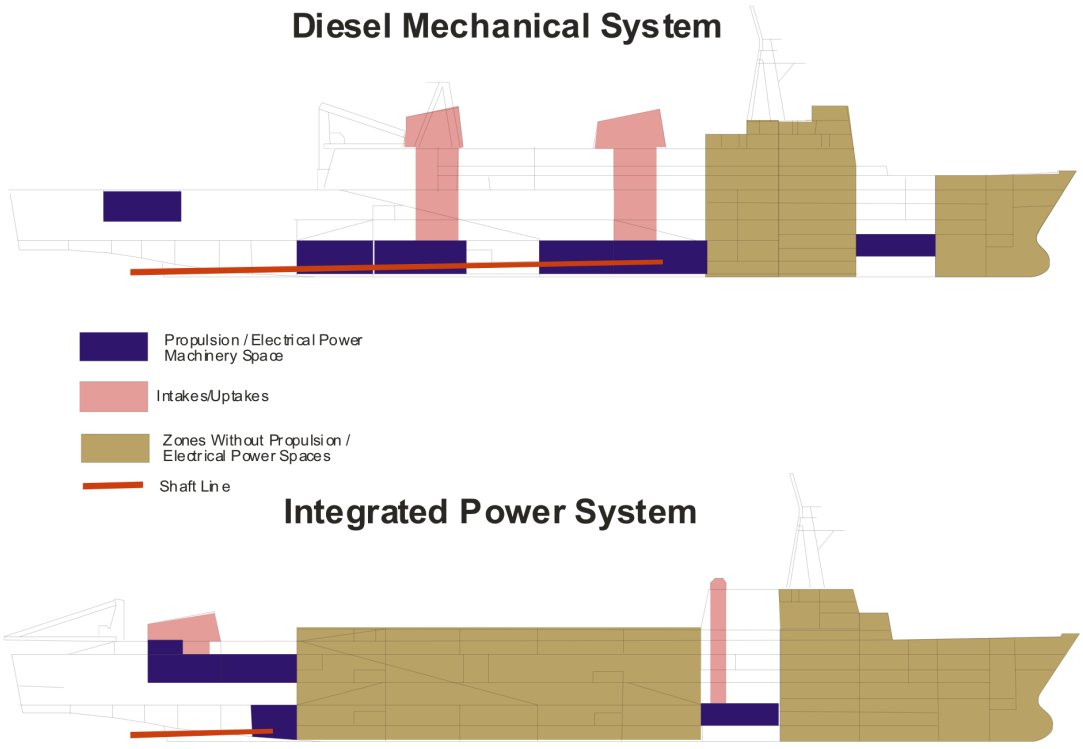

Figure 3. Weight Distribution Model Comparison for a Traditionally-Powered Ship and a Ship Using an Integrated Power System. From [2]

pods can physically spin 360 degrees, allowing the direction of thrust to influence the ship's course, instead of using a rudder [1]. This also eliminates hull penetration that a shaft creates when transferring energy from inside to outside the ship.

III. ELECTRIC MOTORS

When a ship employs an integrated power system, the most noticeable change is that the propulsion is no longer powered from a generator through reduction gears, as in a segregated system. Instead, an electric motor is used to convert the electrical energy from the power grid into torque to turn a propeller shaft. Electric motors convert electrical energy into mechanical energy by using interactions between magnetic fields that oppose one another in a form that can produce torque. The magnetic fields are created either by current carried through coils of conductors, like a solenoid (Figure 4), or permanent magnets. These currents can be powered by DC power or AC power, leading to different designs, each with its own advantages and disadvantages.

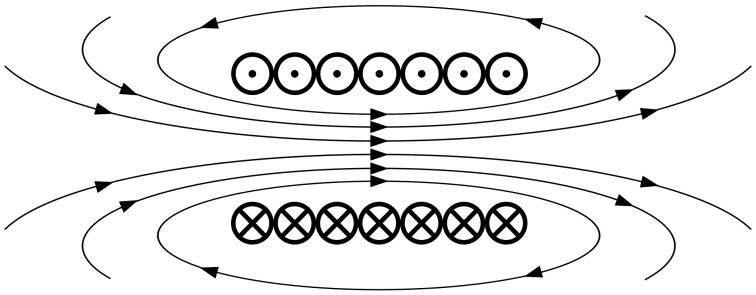

Figure 4. Simple Solenoid. Circles with dots represent current into the page, and circles with xs represent current out of the page. Field lines represent magnetic fields. From [6]

A. DC MOTORS

In its simplest form, a DC-powered motor, shown in Figure 5, provides current to a coil of conducting wire, called an armature. That current interacts with oppositely-polarized, permanent magnets that create a magnetic field through the armature. The interaction between the current and the perpendicular magnetic field

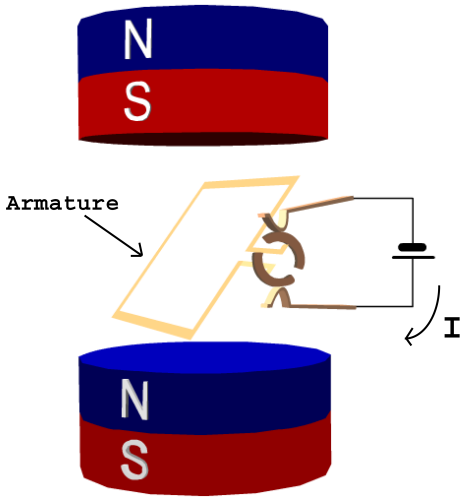

Figure 5. Simple DC Motor Design. After [7]

creates a force by the Lorentz force law $\boldsymbol{F} = I\boldsymbol{L} \times \boldsymbol{B}$, where $\boldsymbol{L}$ is the directed length of the wire, I is the current through the wire and $\boldsymbol{B}$ is the magnetic field vector. The magnetic force that is imposed on the wire results in a torque that spins the armature, and can spin a shaft attached to it. Since the current is in one direction and the magnetic fields do not flip, this type of design requires metal brushes that allow the current to alternate directions to maintain torque in the correct direction. The magnitude of the torque changes in the armature, going to zero when the magnetic field aligns with the plane of the armature. This alternation, or jumping, results in torque fluctuations, and is not ideal in a motor. Homopolar motors avoid this.

1. DC Homopolar Motors

The basic design of a homopolar motor, seen in Figure 6, is a stationary permanent magnet positioned near a current-carrying, rotating disc. The current travels through the disc from the center to the brush contact at the outside of the disc. The interaction between the magnetic field and this current creates a Lorentz force which rotates the disc. Since the brush is always in contact with the rotating

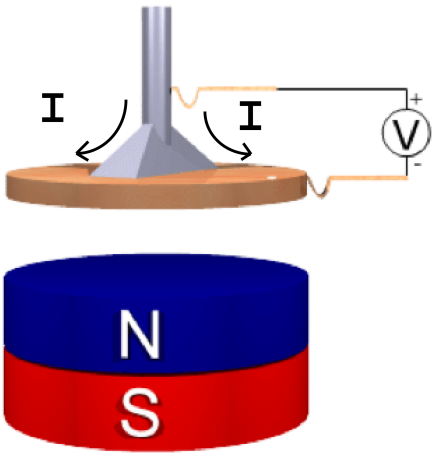

Figure 6. Simple DC Homopolar Motor Design. After [7]

disc the current is constant. The advantage of the constant current, and thus constant torque, is an acoustically quiet motor, because the jumping that occurs in a simple DC motor no long exists [1].

2. DC Superconducting Homopolar Motors

The Navy has long investigated the use of a homopolar DC motor of a superconducting type. The Navy first tested a superconducting DC homopolar motor (SDCHM) in 1980 on the *Jupiter II* test craft, which used high temperature superconducting (HTS) windings of Bi-2223 (a ceramic type HTS material consisting of Bismuth, Strontium, Calcium, Copper, and Oxygen) that operated at liquid Helium temperatures of 4.2 Kelvin (K) [8]. Currently, General Atomics is developing a SDCHM that could be used for shipboard propulsion in future electric ships, seen in Figure 7 [1].

This design would be advantageous for use in future electric ships for the obvious reason that it provides a drastically lighter motor than an AC power equivalent. A benefit that could be seen further down the road would come from advances in IPS technology. If the power grids in electric ships eventually reach the proposed Medium

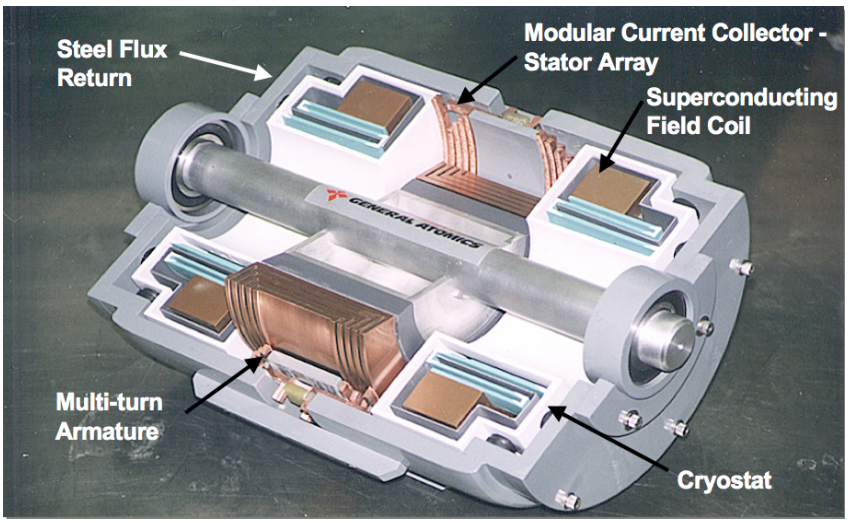

Figure 7. DC Superconducting Homopolar Motor by General Atomics. From [9]

Voltage Direct Current (MVDC) of 6kV, then the electrical power wouldn't have to be converted, as is necessary for an AC motor, further saving weight.

B. AC MOTORS

An AC motor, a simple version of which is seen in Figure 8, consists of two basic parts. The stator is the stationary portion that, in a simple design, lies outside a rotating inner portion called the rotor. When the rotor spins, it transfers the torque it experiences to a shaft. The stator is the portion that receives the AC current, circulating it through its coils of conducting wires. These coils, positioned circularly around the rotor, create rotating magnetic fields that change a specific frequency, dependant upon the current put into them. These fields then interact with the magnetic field of the rotor. There are two types of methods to produce magnetic fields on the rotor. One is a field wound rotor, where coils of conductive wire are wrapped around the rotor which, when supplied with current, creates a magnetic field. The other is a permanent magnet rotor, where permanent magnets are positioned on the rotor to provide the magnetic field. When the fields attempt

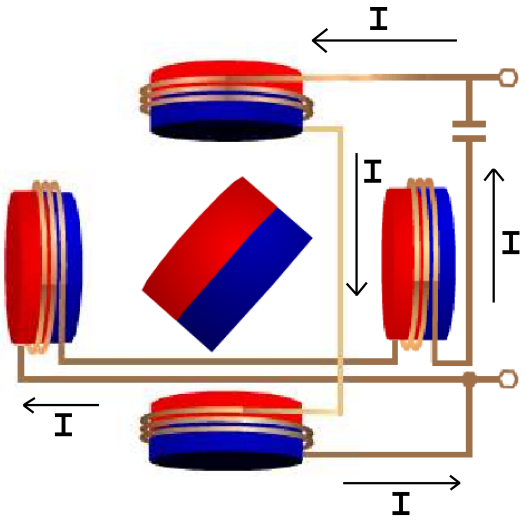

Figure 8. Simple AC Motor Design. After [7]

to temporarily align there is a torque applied to the rotor, which creates the desired rotation. This is accomplished through two types of rotating frequencies that the rotor will encounter.

1. AC Synchronous Motors

In the first type, the rotor spins at the same frequency, or a submultiple thereof, of the rotating magnetic field circulating stator. This is called a synchronous motor. The design favored for a synchronous motor for Navy electric ships has a permanent magnet rotor because of its lower weight [1].

2. High Temperature Superconducting AC Synchronous Motors

In 2009, Northrop Grumman and American Superconductor, under an Office of Naval Research contract, successfully tested a HTS AC synchronous motor (HTS ACSM), seen in Figure 9. The 36.5MW (or 49,000 horsepower) propulsion motor is the most powerful electric motor ever tested by the Navy [10].

Higher power and smaller size result from using HTS wires instead of copper

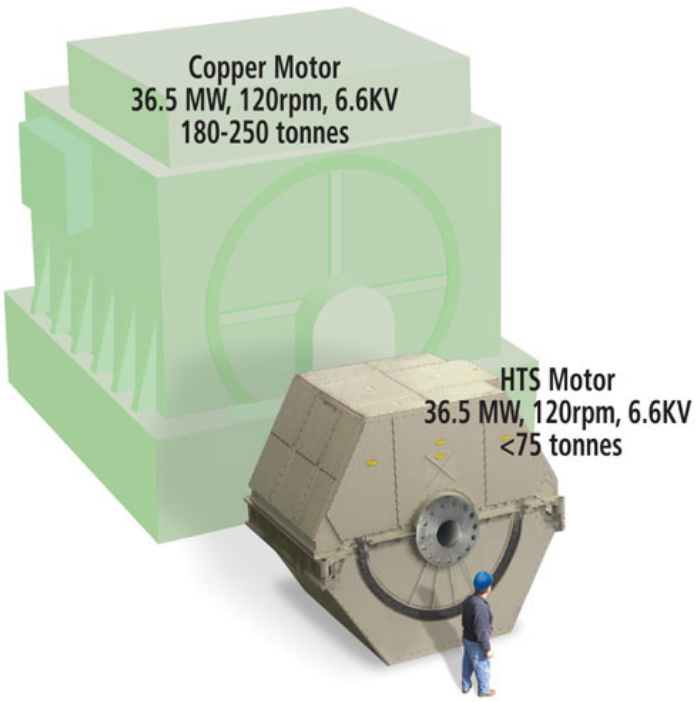

Figure 9. High Temperature Superconducting AC Synchronous Motor by American Superconductor. From [10]

wires in the coils. HTS wires, made from the same ceramic material Bi-2223 described before, can carry up to 140 times more current than a copper wire of comparable size [11]. And unlike previous superconducting wires that only operate at around 4K, the HTS wires can now operate at a much higher and more practical temperature, somewhere between 25K and 35K [1]. Size and weight point to the use of HTS ACSMs for electric ships in the future.

3. AC Induction Motors

The second frequency at which the rotor can operate in an AC motor is slightly lower than the frequency of the rotating magnetic field. This is called an induction motor. The fractional amount by which the frequency lags behind is called slip (S),

$$S = \frac{n_s - n_r}{n_s} \tag{III.1}$$

where n_s= rpms of the stator's rotating magnetic field, n_r= rpms of the rotor.

The slip determines how fast the rotor will turn, and therefore how fast the shaft spins. An induction motor has conducting windings around its rotor. When the stators magnetic field rotates, it induces a current in these rotor windings. The induced current creates a secondary magnetic field that via its interaction with the stators field causes the rotor to move. A simplified version of this interaction is seen in Figure 10. Since the induced currents depend upon the changing magnetic flux through the rotor windings, the rotor can never spin as fast as the rotating stator field (hence the slip alluded to earlier). As a result of its design, an induction motor can change its rotor spin rate by changing the magnitude of the current through the rotor windings, which changes the slip parameter. This is an advantage over a synchronous motor where the rotating magnetic field must be changed, providing one advantage in use of induction motors.

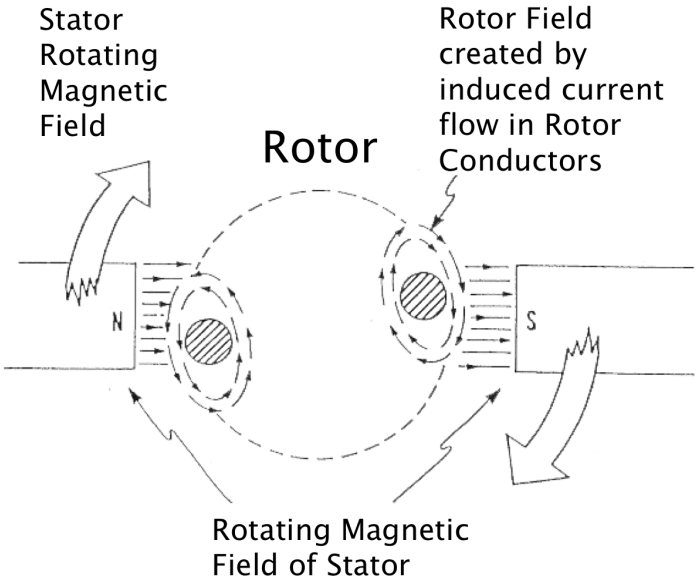

Figure 10. Simple AC Induction Motor Design. After [12]

The Navy has favored this type of motor for the DDG-1000, mainly because the previously favored AC synchronous motor was delayed due to design issues from DRS Technologies. The advanced induction motor that will be on the DDG-1000 is built by Converteam, seen in Figure 11 [13].

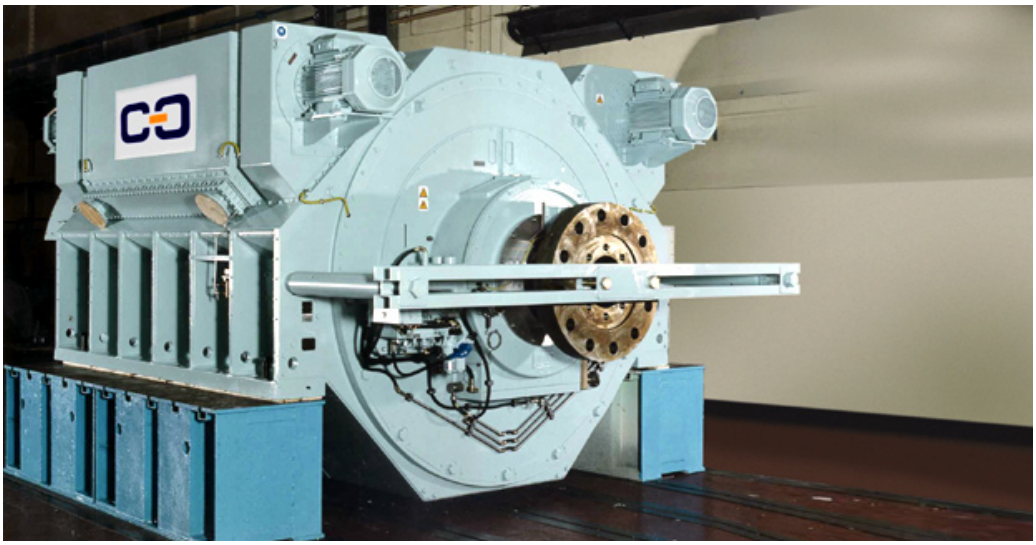

Figure 11. AC Induction Motor by Converteam. From [13]

IV. THE FREE ELECTRON LASER

"Light Amplification by Stimulated Emission of Radiation," or LASER, is a process by which coherent electromagnetic radiation is created. A conventional laser uses a highly reflective optical cavity that encloses a gain medium inside. Once the gain medium is "pumped" via some external supply of energy, it can amplify light that is passed back and forth through it. Some of the light then escapes from a partially transmissive mirror at the end of the cavity. One defining quality of a laser is the makeup of the gain medium; most media are either a gas, solid, or liquid. In all these conventional cases, the process by which the material lases is the excitation of electronic or molecular states in the medium. As the molecules transition back to lower energy levels, they transfer their excited-state energy into a radiation field. Since the transitions between excited states are discrete, with energy spacings dependent on the gain medium, wavelength is more or less fixed for a gain medium. An example of these transitions of electrons from lower states to higher states, and back down is shown in Figure 12. This feature is relatively unattractive

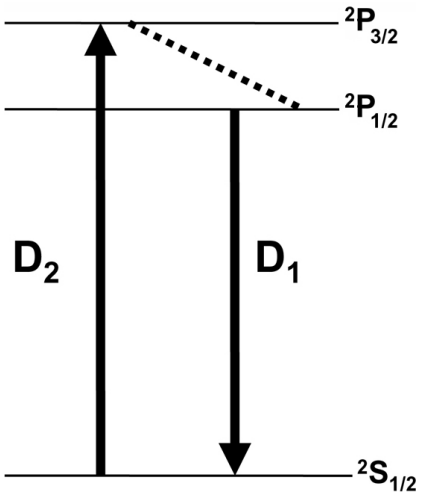

Figure 12. Electron Energy Transitions. From [14]

to the U.S. Navy since changing atmospheric conditions may dictate wavelengths not attainable from conventional lasers, especially at the output power needed for defensive applications.

The Free Electron Laser (FEL), invented in 1971 by J.M.J. Madey at Stanford University, is similar to a conventional laser, namely it also provides a beam of coherent light through a stimulated emission process. The key difference between an FEL and a conventional laser is that an FEL uses a relativistic electron beam as its gain medium.

Figure 13 shows a basic layout of an weapons-class FEL design. The system starts at the injector where a cathode emits a pulsed beam of free (unbound) electrons. The electrons in each pulse have a natural tendency to spread out due to Coulomb repulsion. To counter this effect, the injector quickly accelerates them to

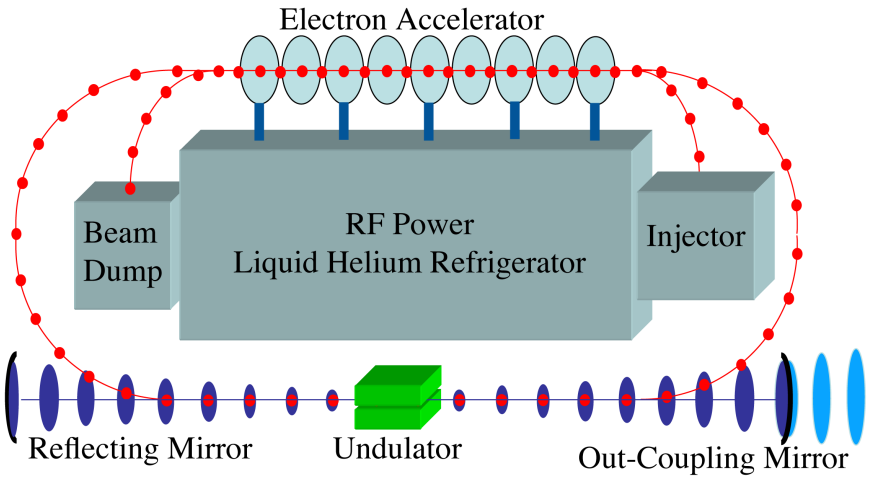

Figure 13. Basic Free Electron Laser Design. From [15]

relativistic speeds and energies of a few Mega-electron-volts (MeV), which minimizes the spreading. After the initial acceleration by the injector, the electrons move down the beam pipe to the radio frequency (RF) superconducting linear accelerator (linac), which uses RF waves to accelerate the charged electrons. The linac operates at liquid

helium temperatures, so it requires large amounts of power, both to keep the cavity cold and to accelerate the electrons up to 100MeV [15].

Upon leaving the linac at high energy and relativistic speeds the electrons enter the undulator, or wiggler, which uses a series of magnets with alternating poles to create magnetic fields in the laser cavity. The alternating magnetic field causes the electrons to accelerate, through Lorentz force interactions, and then emit electromagnetic radiation. Feedback between the electron and light pulses create coherent radiation in the beam as a consequence of bunching within the electron beam. The newly created light is then reflected back and forth in the optical cavity with a fraction out-coupled on each pass through the partially transmissive mirror. If the beam director does its job, the next stop is the target.

In addition to this device, which would be described as an oscillator FEL, there is another FEL which amplifies light from a seed laser of relatively low power. Amplification occurs in the undulator in a similar manner as before, namely the bunched electrons impart energy onto the light and amplify it to higher power. But in this case, the amplifier FEL, the light beam does not reflect between mirrors; it makes a single pass through the undulator.

After the electron beam passes through the undulator, it could be disposed of. However, this would be wasteful, since only a small amount of electron energy is converted into light. Instead, the electron beam can be recycled back to the beginning of the linac, but now out-of-phase with the RF, so that the beam is decelerated, thereby recovering much of the energy. This is called an energy recovery linac (ERL). The Navy would be inclined to use an ERL since power on a ship is limited to what its power plant can generate, typically around 100MW.

Another advantage of an ERL is the reduced radiation hazard. The power in the electron beam has to go somewhere to slow down and this takes place at the beam dump. A problem, however, occurs when electrons have energy and are rapidly decelerated called Bremsstrahlung radiation, making high-energy photons. Neutron

radiation should be minimized and since Navy crew will be near the FEL on a ship and radiation cannot affect their persons. If the ERL process is being used, not only is invested energy reused, but the energy of electrons going to the beam dump is reduced to safe levels.

As mentioned before, a detractive quality of conventional lasers is that in general they can only operate at fixed wavelengths. An FEL, however, avoids this restriction since its gain medium does not produce light based on discrete excited state transitions, as in a conventional laser. The wavelength of an FEL is determined by two main parameters, the undulator period, the dimensionless undulator parameter, K, and the electron beam energy. It is governed by the equation

$$\lambda = \frac{\lambda_0(1 + K^2)}{2\gamma^2}, \tag{IV.1}$$

$$\text{where } K = \frac{eB_{rms}\lambda_0}{2\pi mc^2},$$

where K =undulator parameter, λ_0 =undulator period, γ =Lorentz factor, so that the electron kinetic energy is $T = mc^2(\gamma - 1)$, m is the electron mass, and c is the speed of light. This relatively simple equation shows that there is a wide range of wavelengths achievable from an FEL, assuming that the parameters needed to produce it are attainable.

In conventional lasers, the amount of pumping that is done to the gain medium, in order to excite electrons into higher states, is what determines the power of the laser light output. Unfortunately for most gain mediums, there is a limit to how much power can be put into the gain medium before the medium is damaged or distorted. An FEL does not suffer from this problem because of its use of electrons as the gain medium.

Current proposed FELs to be placed on electric ships are aimed at having a peak output power at the Megawatt level. They are intended to target inbound missiles traveling at supersonic speeds out to ranges of about 10 kilometers (km). The

use of light instead of bullets to shoot down missiles provides significant improvement from the current Phalanx Close-In Weapon System (CIWS), shown in Figure 14. The first advantage is that light almost instantly arrives at the target, traveling at 3.00×10^8 meters per second (m/s), whereas the bullets from a Phalanx CIWS only leave with a muzzle velocity of around 1,100m/s giving the missile more time to close distance to the ship. The other distinct advantage is the range of 10km for an FEL [15]. While the range for the Phalanx CIWS is classified it is difficult to compete with the accuracy of a light beam at long ranges because of bullet pattern spreading and the range of engagement lost while the bullets travel to meet the missile. With decreased

Figure 14. Phallanx Close-In Weapons System (CIWS). From [16]

power output, FELs could also damage and disable small watercraft and aircraft. This advantage is due to its small beam width and pinpoint accuracy, which allows it to produce extreme damage in targeted spots, surgically. That, factored in with the capability of running twenty four-seven, means that the FEL will revolutionize Naval-ship defense systems.

THIS PAGE INTENTIONALLY LEFT BLANK

V. THE FREE ELECTRON LASER MODEL

The model created for the FEL involved a great deal of collaboration. Using collective ideas from NAVSEA, Stanford, Advanced Energy Systems, and Jefferson Lab, and NPS, the appropriate design parameters, engagement scenarios, and states of readiness were determined. This information was then used to design a model at the University of Texas at Austin's (UTA) Center for Electromechanics (CEM). Created in Simulink®, a modeling tool that integrates into MATLAB^{TM}software, the model was designed to estimate the power demands at different states of readiness, how the

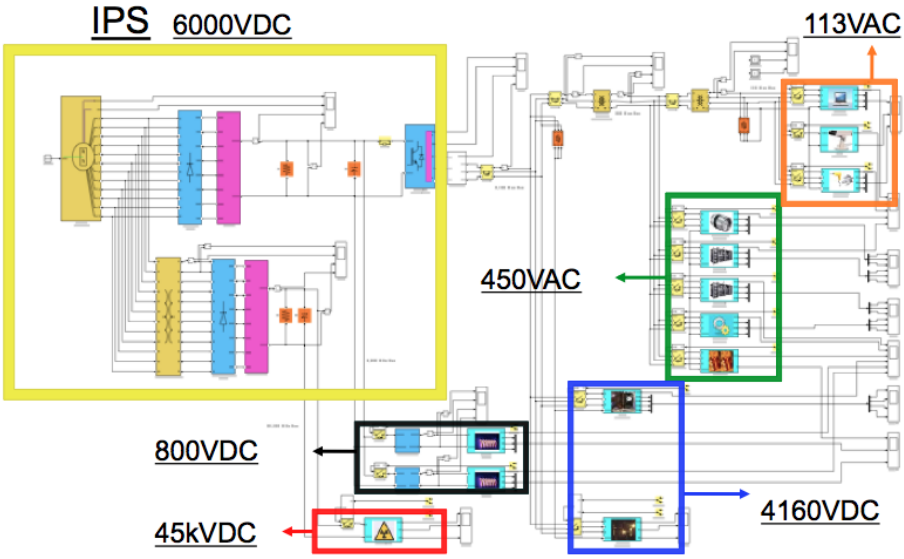

Figure 15. Simulink Model of FEL Simulation on an Electric Ship

electric ship handles the transitions between these states, and the transient loads on the power grid. A diagram from Simulink is shown in Figure 15 that nicely lays out the voltage buses available on the electric ship, both AC and DC, and the components that draw from those buses. The voltages to be included are 600VDC, 4160VDC, 45kVDC, 113VAC, and 450VAC. The components on those buses are outlined in colored boxes in Figure 15.

The FEL model shown in Figure 16 does not specify a particular FEL design but rather a notional weapons-class FEL that could be used aboard a future electric ship. The software model can be later adjusted to better represent the new FEL designs as they emerge.

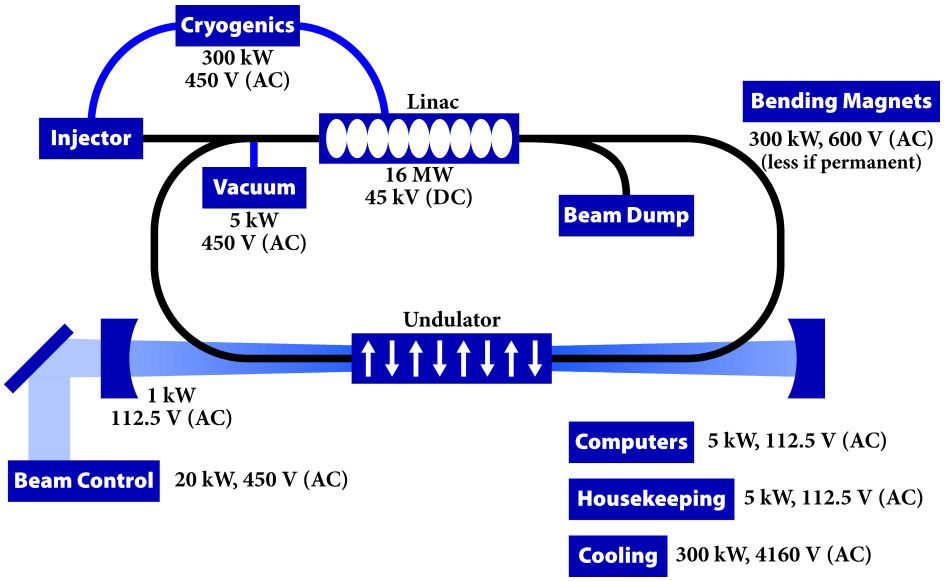

Figure 16. FEL Model Components

To better understand the model overall, the design and power requirements of each major FEL system will be described in more detail.

A. SYSTEM DESCRIPTIONS

1. Cryogenics System

The superconducting cavities used in the injector and linac of the FEL must be able to operate at 2K and 4K, which requires liquid helium. The power requirement depends on both the heat load and on the refrigerator efficiency. The heat load is made up of two components. The static component is from heat leakage into the cryogenic lines and liquid helium storage vessels, and the dynamic component is from

RF resistive losses in the linac and injector. A recent estimation predicts 300kW of power to run the cryogenics with a 0.1% refrigerator efficiency.

2. Cathode

The cathode is the source of electrons for the FEL electron beam. When a drive laser focuses its light onto the cathode, electrons are emitted through the photoelectric effect. The photocathode yields an average electron current of ∼1 Ampere (A) accelerated across a potential of 500kVDC for an average power of 500kW. The electron beam is pulsed, but the pulses are on the order of nanoseconds apart, so the beam is treated as a continuous beam in the model. The cathode is indistinguishable from a constant, continuous load on the power grid.

In addition to the cathode power requirement, this system also requires small amounts of power to other systems like the drive laser. These do not change the model significantly so they are excluded from calculations. At present the photocathode power usage is not included, but it will be in future models.

3. Injector and Linac

After the electrons are emitted from the cathode, they are accelerated to relativistic speeds by the injector. This energy is difficult to reclaim in the energy recovery portion of the beam path. The electrons must be accelerated to relativistic energies in the injector to reduce space charge effects that would degrade the beam too much before entering the linac.

After leaving the injector the linac accelerates the electrons to highly relativistic energies, approximately 100MeV. The model assumes an energy recovery linac will be used, so that most of the energy put into the electrons by the linac will be recovered when they return to the linac out of phase. This makes the linac much more efficient.

Both the injector and the linac are driven by a shared RF source consisting of either klystron banks or inductive output tubes operating on the 45kVDC bus.

Power requirements from the RF source depend on factors such as efficiency of AC to DC and DC to RF conversions, accelerating cavity properties, and electron beam configuration. It is estimated in the model that the RF source will need roughly 16MW of power.

4. Beam Dump

After the electrons have been used in the undulator to create laser light and have been recycled through the linac, and stripped of recoverable energy, they are still energetic and must be properly dumped. The beam dump takes the energetic electrons and lowers their energy by converting the energy to large amounts of heat and radiation.

The proposed method of removing this heat involves pumping water through channels in the beam dump. This can either utilize existing onboard water cooling, or will require small amounts of energy compared to the other systems.

5. Other Loads

In addition to the larger loads already described for the main systems of the FEL, there are also smaller loads for several other components. The magnets that steer the beam inside the vacuum-sealed beam line are directed by two methods. One option uses permanent magnets that steer the beam with actuators that physically move the magnets for small adjustments in beam path. The second option is electromagnet-controlled steering, where the strength of the magnetic field from quadruple and dipole magnets fine-tune the beam path. The estimated total power for the magnets is ∼300kW on the 6000VDC bus.

Although the majority of the cooling is needed to cool the accelerator cavities and the RF source, there is also a need for cooling to ensure that all the other FEL components operate at safe temperatures and avoid thermal damage. The power demand for this additional cooling is estimated to be ∼300kW on the 4160VAC bus.

The power demand for the beam control, which directs the FEL light output

to the target and includes an adaptive optics feedback system, is estimated to be ∼20kW on the 450VAC bus.

Since the entire beam path and cryogenic lines are held in a vacuum state, ∼5kW on the 450VAC bus is necessary to power the pumps that keep the system in vacuum.

Computers and other miscellaneous housekeeping items are estimated to take ∼5kW of power each, ∼10kW total, on the 113VAC bus. Other optical systems and actuators come to 1kW on the 113 VAC bus as well.

There are also systems for which an unknown power may be needed. The fire control system that handles target acquisition and tracking, similar to what already exists with the Phalanx CIWS, will need to be included, as will vibration suppression, which will isolate sensitive optical alignments from the ships constant vibrations. Neither will be large loads and are not included in the model presently.

B. STATES OF READINESS

Since power is a costly commodity aboard a ship, leaving all FEL components at full power would draw too much power and waste too much fuel, as well as causing unnecessary and undesired aging to some of the components. For this reason, different states of readiness have been created for the FEL, ranging from the ship being tied up pier side to the FEL shooting during engagement. Each state of readiness is designed to coincide with the perceived threat level that the ship is encountering at that time and how long it should take the FEL to be able to fire. The different states have different power draws that best suite its conditional readiness, and the five states are listed in Table I.

It is noted that each state of readiness has conditions for components that designate them as off entirely, at a partial power draw, or full power draw. There are a few components that are never turned off or lowered in power draw for any states of readiness, unless those systems are undergoing repairs.

States of Readiness			
State	Description	Power	Transition Time From Previous State
Pier Side	FEL in minimal power state necessary maintenance performed	425kW	Days
Underway	Ship is crossing open water; no imminent threat	625kW	Hours
Hot Standby	Ship is in combat theater; threat could appear at any time	1MW	Minutes
Engagement	FEL is firing upon incoming threat	17MW	Seconds
Operational Readiness Between Shots	FEL is between shots; additional threats still inbound	17MW	Milliseconds

Table I. FEL Model States of Readiness Summary

To provide an easy visual aid in seeing which power systems are at full draw, partial draw, and off, each state of readiness has a color-coded diagram. Components colored in green are fully powered, yellow are partially powered and red are off.

1. Pier Side

The first state of readiness is pier side (Figure 17) where the ship would be tied up in a port with no likely threat perceived. This is the state that requires the least amount of power since several of the components are at a minimum power draw and other components are off entirely. Components that are off at this state are the components that are only needed when the electron beam is circulating in the system; bending magnets, and beam control.

The components that are at a low power state are those that take long periods of time to fully turn on. One of those components is the cryogenics, since it takes several days to cool the accelerating cavities and cryogenics from room temperature to operational temperatures. If the cryogenics are kept at 4K instead of 2K, it takes significantly less power to maintain (100kW instead of 300kW), and only takes a few

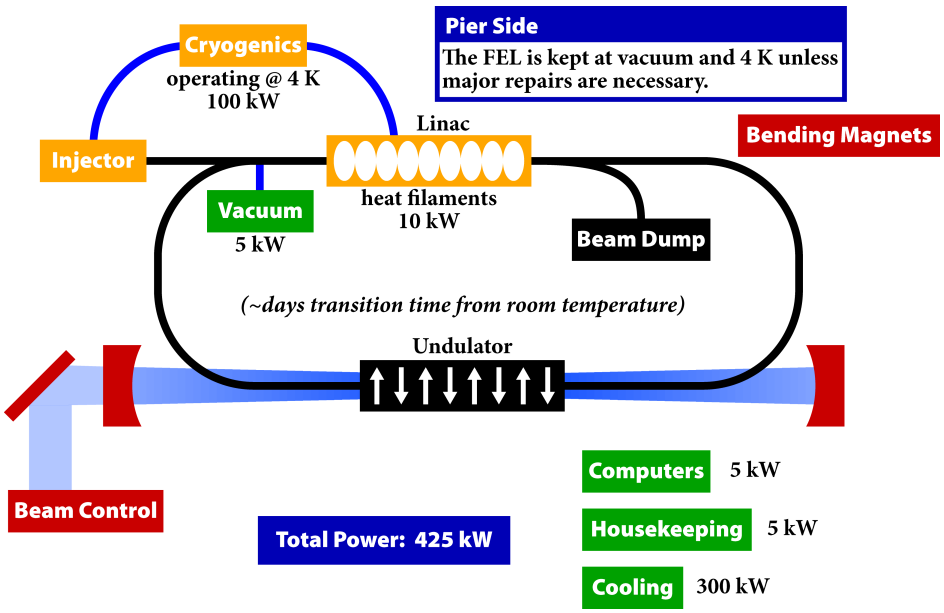

Figure 17. FEL Components at Pier Side State of Readiness, with Power Draws

hours to transition to 2K – a feasible time frame for getting underway quickly.

Another component that receives partial power due to its long turn-on time is the RF source for the injector and the linac. To make what would be a several hour transition much shorter, the RF filaments are kept at a lower power state that draws about 10kW.

As mentioned, there are components that are almost never turned off or lowered in power draw. The pumps that keep the beam line and components at a vacuum state is fully powered, with only a 5kW draw. The various other systems that are needed for the FEL, such as computers that run the systems, various housekeeping and cooling all stay on at a little over 300kW of power altogether.

The total draw at pier side is around 425kW, and could come from shore power when the ship is tied up, rather than the ship's generators. From the pier side state of readiness, the FEL can become fully operational in just several hours.

2. Underway

The next state of readiness, which takes several hours to reach from the pier side state, is underway (Figure 18). At this state the ship is traveling on open seas with no potential threat in the immediate area. However, the possibility of needing the FEL within several minutes, for testing the device or in the event of a threat moving in the vicinity, forces the system to operate at a higher power draw than at pier side.

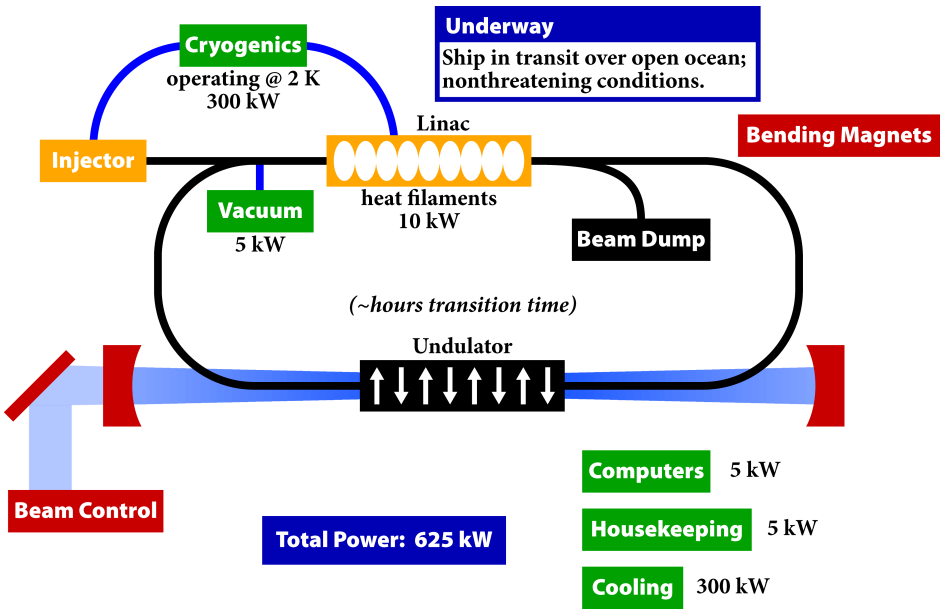

Figure 18. FEL Components at Underway State of Readiness, with Power Draws

The only change from the pier side readiness state is the cryogenics are cooled from 4K to 2K to reach operational temperatures for the injector and linac. This lowering of 2K raises the power demand from 100kW to around 300kW total for refrigeration. This shifts the total power draw from 425kW to 625kW, and now the FEL is ready to operate the electron beam for the next state of readiness. The time to firing capability is now just several minutes.

3. Hot Standby

When the ship moves into the combat theater and potentially faces a threat, it must be able to fire the FEL in under 1 second. A balance between fully powered and efficiently powered is reached in the state of operational readiness for the FEL (Figure 19). Since the need to quickly turn on the FEL requires that the electron beam reach full circulation current quickly, this system needs to be prepared. So a

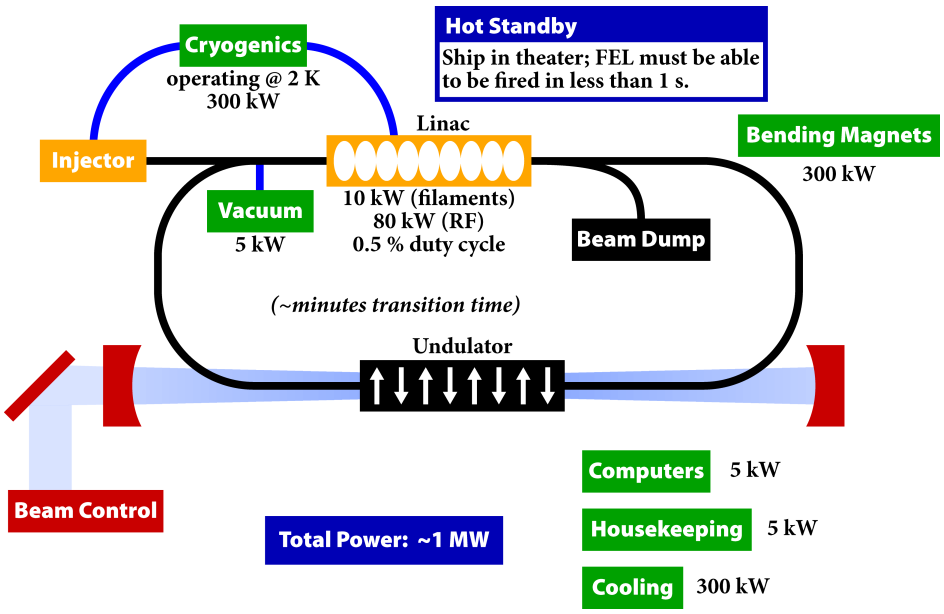

Figure 19. FEL Components at Hot Standby State of Readiness, with Power Draws

lower average current, and thus lower average power, is used. There must be enough electrons circulating to achieve and maintain both alignment of the electron beam and saturation in the optical cavity, so a fractional duty cycle is used in the linac. The bending magnets must now be turned on to direct the beam and maintain alignment, which takes around 300kW of power.

Using a fractional duty cycle circulates electrons for only a few microseconds, allowing the steering magnets to adjust and be prepared for full beam. To achieve this the injector only fills every 200th RF cycle with electrons (or about every 200ns)

giving the RF cavity a fractional duty cycle of 0.5%. This only requires 80kW of power to run – much lower than the 16MW for full circulation. Another mode of operation would be to run the electron beam at full duty cycle, but only about 1 millisecond out of every second. This would allow the RF fields in the cavity to stabilize without requiring additional power.

The total power used in the hot standby state is around 1MW, a little less than double of the previous, underway state; this state is achieved in just a few minutes.

4. Engagement

From hot standby the ship can fire in under 1 second. The readiness state at which the FEL is firing is the engagement state (Figure 20). At this state, all components are now fully powered and the laser is producing megawatt level light, out-coupled to the target. The changes in power requirements from hot standby are

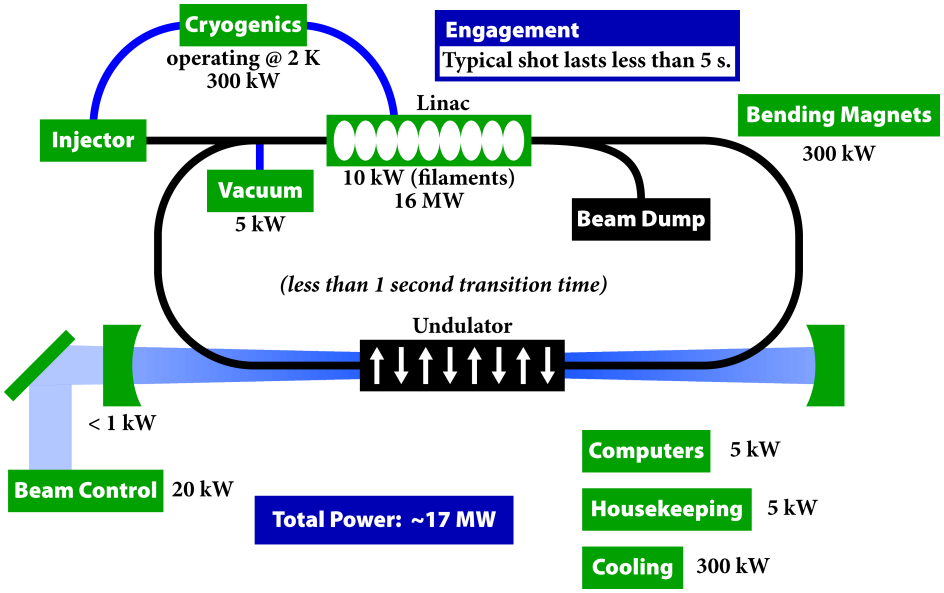

Figure 20. FEL Components at Engagement State of Readiness, with Power Draws

only at the injector, and linac. The injector and linac now operate at full power and

require around 16MW of power to circulate the electrons at maximum current. The entire state now takes around 17MW.

The engagement state is typically only maintained for less than 5 seconds, which is the estimated time to engage a target. The notional model predicts around just 2 gallons of fuel will be burned at the generators to fire for the full 5 seconds. After firing the state of readiness would be reduced to either operational readiness between shots to fire again, or even further down in power demand to hot standby still ready to fire in seconds. This, of course, depends on the threats imminent to the ship.

5. Operational Readiness, Between Shots

The last state of readiness is an optional state that follows engagement named operational readiness between shots (Figure 21). The name of this state implies its

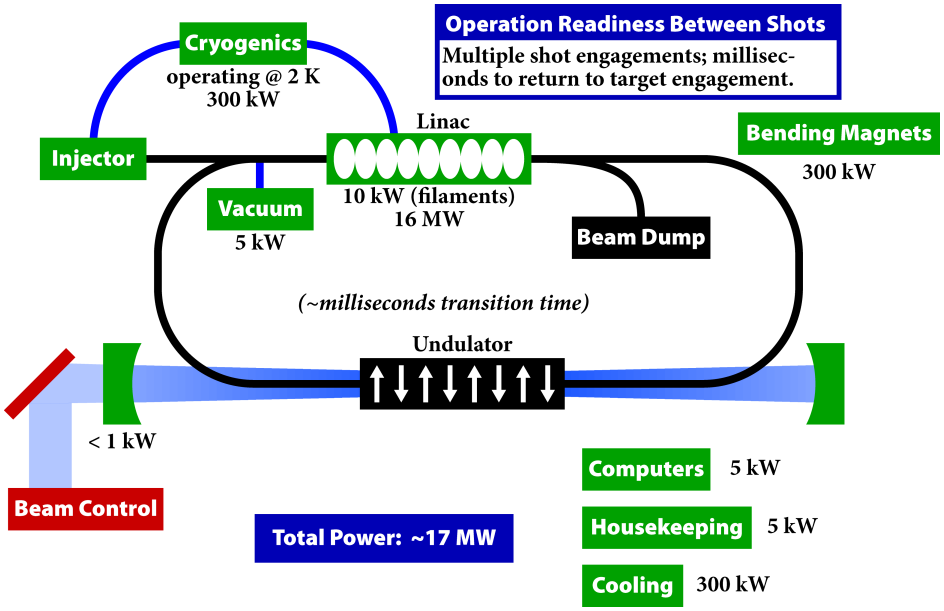

Figure 21. FEL Components at Operational Readiness Between Shots of Readiness, with Power Draws

purpose–this would be a condition set when there is still a threat engaging the ship

and shifting the ship back to hot standby from engagement would be unnecessary. From this state, the FEL is ready to fire again in just milliseconds – essentially instantaneously. The only difference between this state and engagement is the ship is no longer sending laser light out, so every component is fully powered except the beam control. The reason this state is necessary is that sweeping the laser light across the sky to the next target could turn out to be dangerous to friendlies.

Additionally, there would need to be a method to dispose of the laser light still being produced by full beam circulation. One that could be used to shut-off the FEL would be to misalign one optical cavity mirror to keep the system from producing light. The alignment could be quickly regained to produce laser light again in approximately 10μs.

The total power required at this state is the same as the engagement state, 17MW.

C. RESULTS

Using the MATLAB and SIMULINK model that was developed with UTA, the transitions between all states of readiness were run. Each run was either 6 or 12 seconds, depending on the voltage bus of interest during that transition, and took about twenty-four hours to compute. It is important to point out that, due to these long computation times, each run only went through one transition between states of readiness. Each transition was executed when startup transients died down from the generator turning on.

For each transition there were two types of model parameters run, one with adjusted parameters to achieve additional circuit filtering and one without the adjustment, giving two outputs for each transition. The purpose of the second run was to smooth out large amplitude fluctuations observed on the 6000VDC, 4160VAC, 450VAC, and 113VAC voltage buses. The fluctuations resulted from the large series inductance value in the DC to AC converter that took power from the 6000VDC bus

and transferred it to the 4160VAC bus, then ultimately to the 450VAC and 113VAC buses. To eliminate these fluctuations, the series inductance value was changed to 1/10 its original value. This resulted in transitions between states of readiness that saw smoother voltage traces on the aforementioned buses. In all figures, runs where the series inductance was at its original value are labeled as "Non-Smooth" and runs where the series inductance is 1/10 its original value are labeled with "Smooth."

The smoothing that results from the series inductance value change very clearly shows the benefit from modeling these types of systems. In this case, changing something as simple as the series inductance in the DC to AC power conversion results in drastically different amplitude fluctuations for all state-of-readiness transitions. Removing these fluctuations is an important design goal in including an FEL system on an Integrated Power System. If the ship saw any of these voltage fluctuations, significant damage could result to critical electrical components on the ship.

1. Control Run

The first model run was a control run in which the turbine generators are turned on at 0 seconds and run for a total of 6 seconds, with all other components off for the entire run. The purpose of this run was to see how long it took for the startup transients to die out and the system to reach steady-state. Knowing this time is important later when looking at transitions between states of readiness. As seen in Figures 22(a) through 27(b), it takes around 3 seconds for the initial generator transients to die out and to reach steady state in the system. Also noted in these figures is that there isn't any apparent difference between the non-smooth and smooth runs. When no components are turned on, there is no significant power draw from these buses, thus no opportunity for adverse interactions. The first case, seen in Figure 22 show the 6000VDC bus voltage over 6 seconds. After about 3 seconds, the bus reaches full voltage and there is little difference between the non-smooth and smooth cases. Figure 23 shows the 4160VAC Bus RMS voltage output, which is similar to the 6000VDC output and reaches 4160 volts (RMS) after a few seconds.

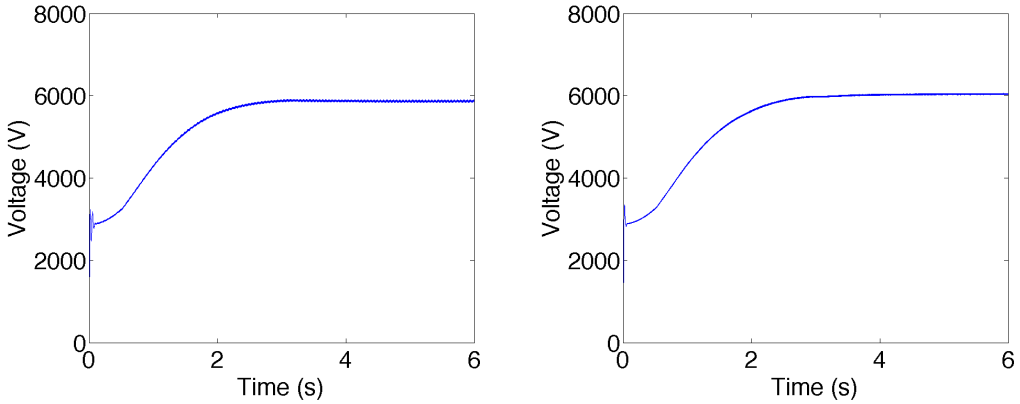

(a) Non-Smooth (b) Smooth

Figure 22. 6000VDC Bus Voltage Output, Control Run

Figure 24 shows the 450VAC bus voltage case, which appear to be a solid blue for the 6 seconds because the fluctuations are so rapid that they blend together. The average voltage alternates between positive and negative 450V, since it is AC power. No visible differences occur between the non-smooth and smooth cases. Figure 25 shows the 113VAC bus voltage case, which again displays the solid color across 6 seconds similar to the 450VAC case, averaging to positive and negative 113V. Figure 26 shows the 45kVDC bus voltage case with no substantial differences between non-

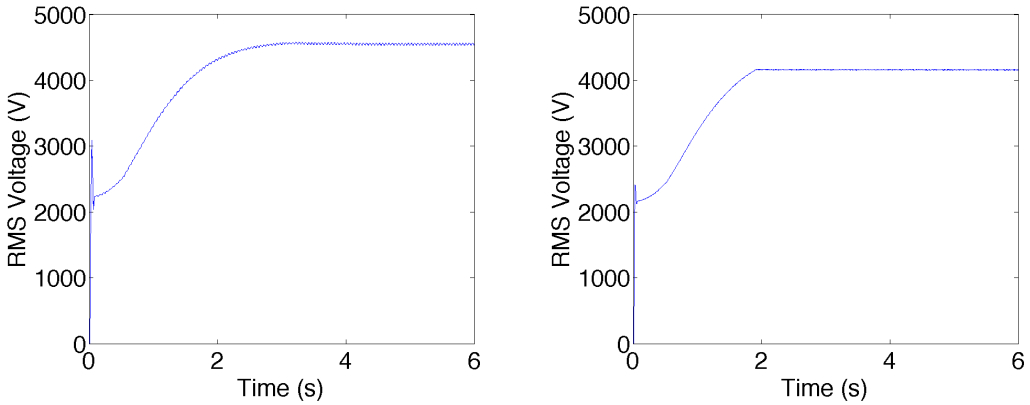

(a) Non-Smooth (b) Smooth

Figure 23. 4160VAC Bus RMS Voltage Output, Control Run

smooth and smooth. The voltage here reaches its maximum value of 45kV after about 3 seconds. Figure 27 is the last case for the control run and shows the 800VDC bus voltage case with no substantial differences between the non-smooth and smooth casess. Since no components are being turned on or off here, after an initial start-up transient the voltage dies to zero.

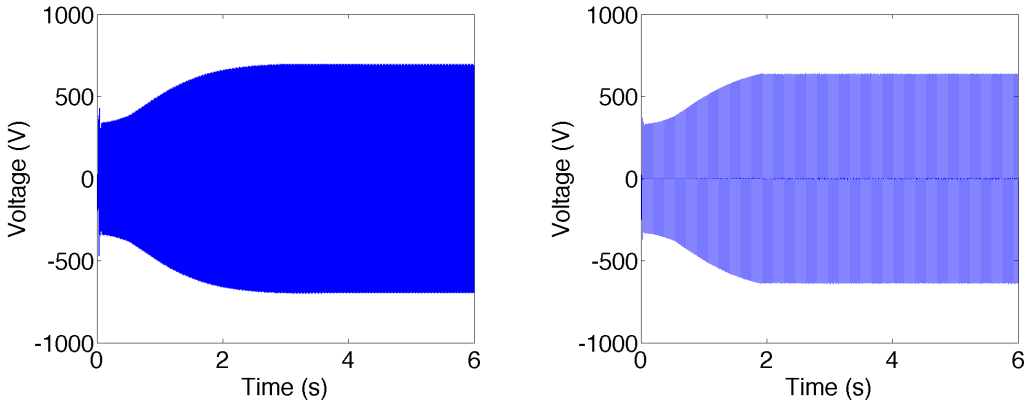

(a) Non-Smooth (b) Smooth

Figure 24. 450VAC Bus Voltage Output, Control Run

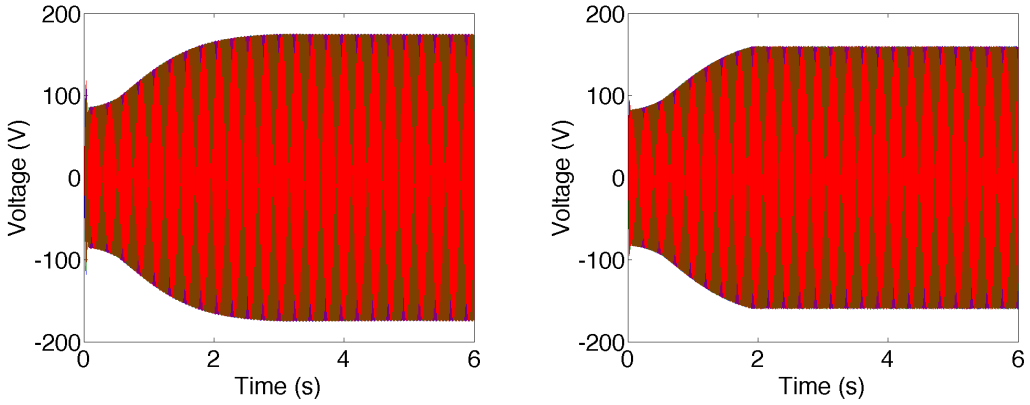

(a) Non-Smooth (b) Smooth

Figure 25. 113VAC Bus Voltage Output, Control Run

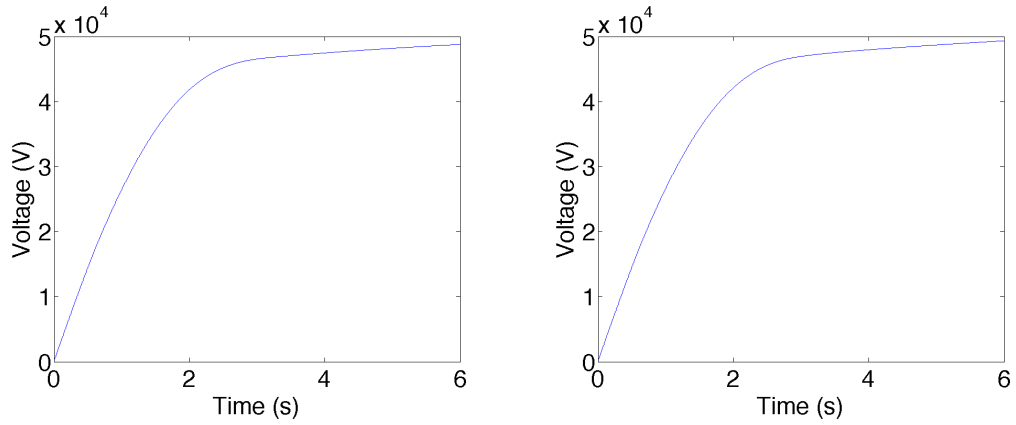

(a) Non-Smooth (b) Smooth

Figure 26. 45kVDC Bus Voltage Output, Control Run

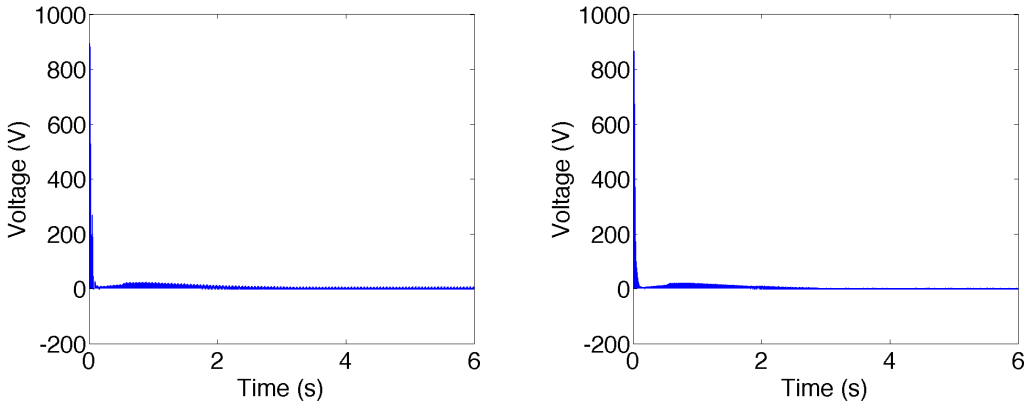

(a) Non-Smooth (b) Smooth

Figure 27. 800VDC Bus Voltage Output, Control Run

2. Pier Side to Underway

The first state-of-readiness transition run was from pier side to underway. At time zero the components that are at full power are the vacuum pumps (on the 450VAC bus); computers, housekeeping, and cooling (all on the 113VAC bus). The components at partial power draw are the RF component's heating filaments and the cryogenics (both on the 450VAC bus).

After 3 seconds, enough time has elapsed for the start up transients to die out and the cryogenics system is boosted to full power to cool the system to 2K. Since the cryogenics system is on the 450VAC bus, the only voltage buses that are affected are the 450VAC, and the buses that it draws power from, the 4160VAC bus and the main 6000VDC bus.

Figure 28 shows the 6000VDC bus voltage output and demonstrates the large amplitude fluctuations centered around 6000V in the non-smooth run that disappear in the smooth run. Figure 29 shows the 4160VAC bus voltage results. When the

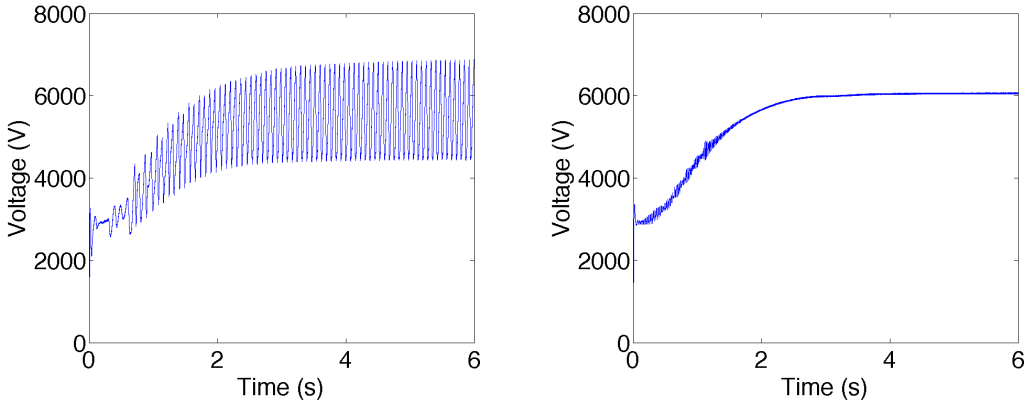

(a) Non-Smooth (b) Smooth

Figure 28. 6000VDC Bus Voltage Output, Pier Side to Underway

transition between states of readiness takes place at 3 seconds the system experiences voltage fluctuations to the already existing envelope of large transients, demonstrating the effect of the high series inductance value on the voltage fluctuations. The smooth case shows the improvement, quickly reaching 4000V with no fluctuations at transition

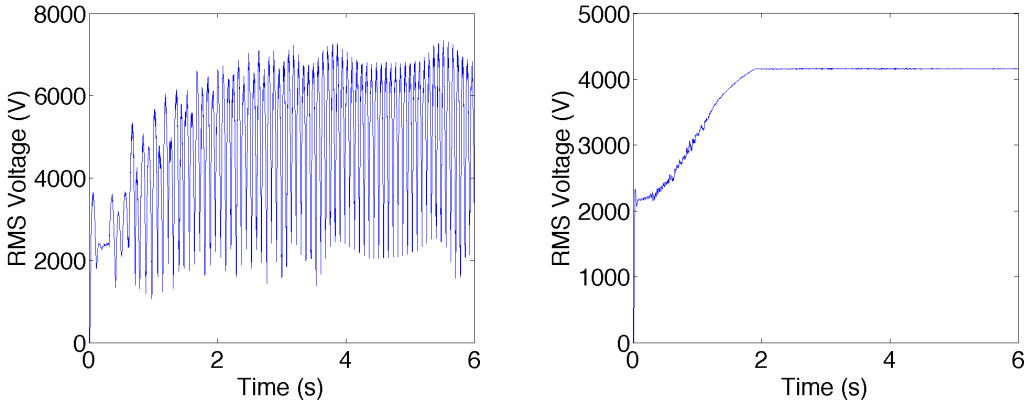

(a) Non-Smooth (b) Smooth

Figure 29. 4160VAC Bus RMS Voltage Output, Pier Side to Underway

time. Figure 30 shows the 450VAC bus voltage results. The non-smooth case shows how quickly the oscillations are taking place between roughly 700V and -700V and sees large transients at transition between states of readiness. The smooth case is

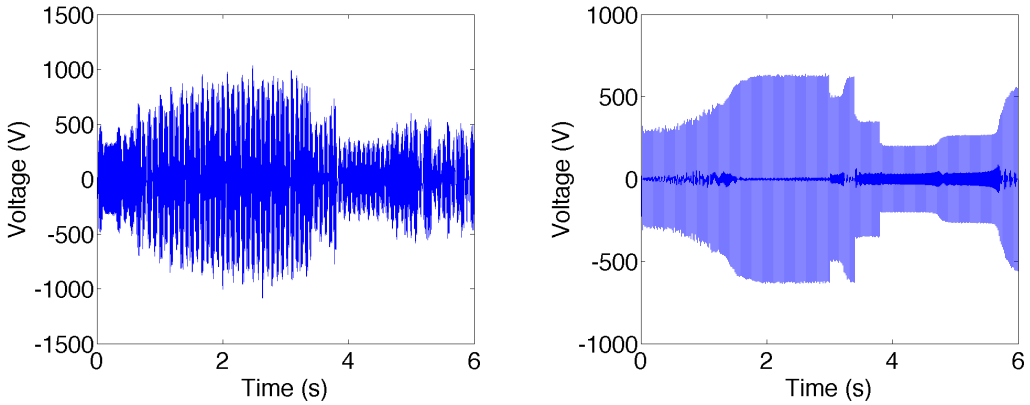

(a) Non-Smooth (b) Smooth

Figure 30. 450VAC Bus Voltage Output, Pier Side to Underway

similar to the non-smooth case but has a more solid color in the voltage due to an overall smoother operation. Trailing off in both cases after 5 seconds the voltage is seen approaching a larger voltage and this is due to delayed turn ons from the refrigerators switching on at 3 seconds. In all of these cases, comparisons between

the non-smooth and smooth results demonstrate the drastic reduction in amplitude fluctuations by lowering the series inductance value in the DC to AC conversion.

All other voltage buses saw no additional transients other than the ∼3 second start-up transients because no components that draw power from those buses were turned on or off.

3. Underway to Hot Standby

The second state-of-readiness transition run was from underway to hot standby. Again, the transition between readiness states takes place at 3 seconds. This transition sees the bending magnets power up (on the 800VDC bus), an increase in power demand from the linac and injector (on the 45kVDC bus).

The only voltage bus outputs that see different transients from the previous transition are on the 450VAC, 45kVDC, and 800VDC buses. The 450VAC bus voltage

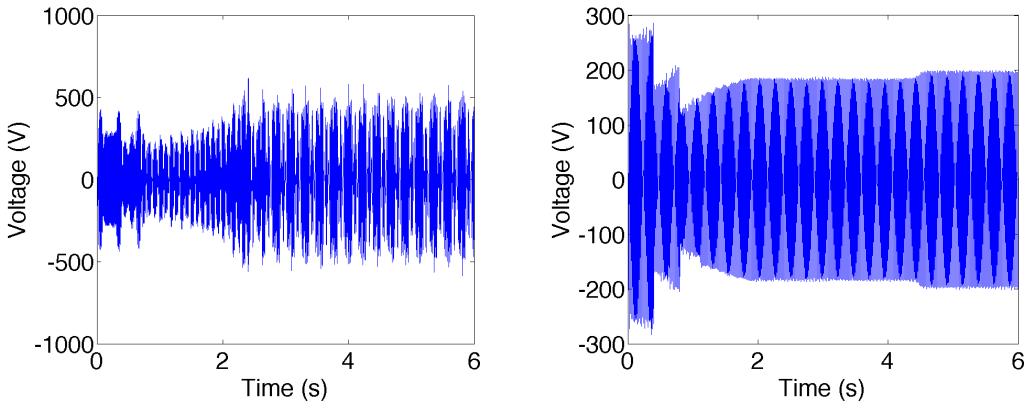

(a) Non-Smooth (b) Smooth

Figure 31. 450VAC Bus Voltage Output, Underway to Hot Standby

output in Figure 31 shows a very choppy result for the non-smooth case, as seen in the equivalent case from the Pier Side to Underway transition. The smooth case is somewhat constant after the transition at 3 seconds, again displaying the solid coloring. Figure 32 shows the 45kVDC bus voltage output and is unchanged from the previous transition. Figure 33 shows the 800VDC bus voltage output. The non-

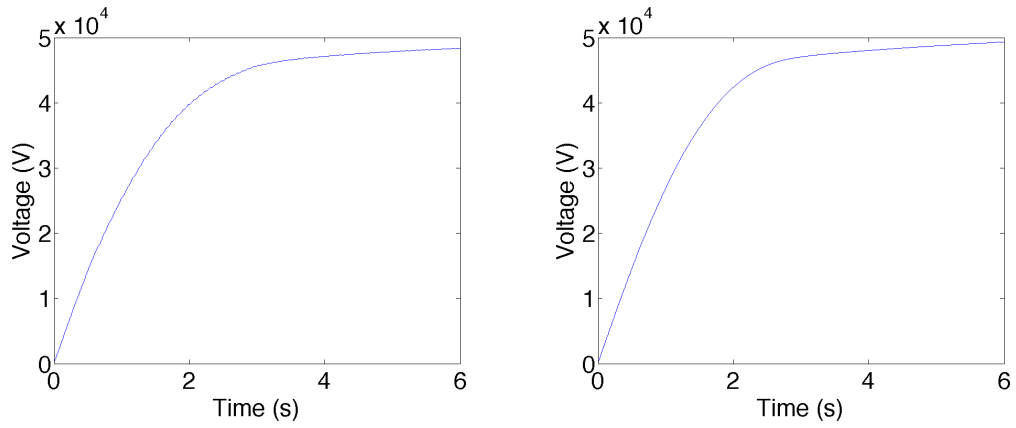

(a) Non-Smooth (b) Smooth

Figure 32. 45kVDC Bus Voltage Output, Underway to Hot Standby

smooth case again suffers large amplitude fluctuations and the does not demonstrate very well what is happening on this voltage bus. However, the smooth case does show

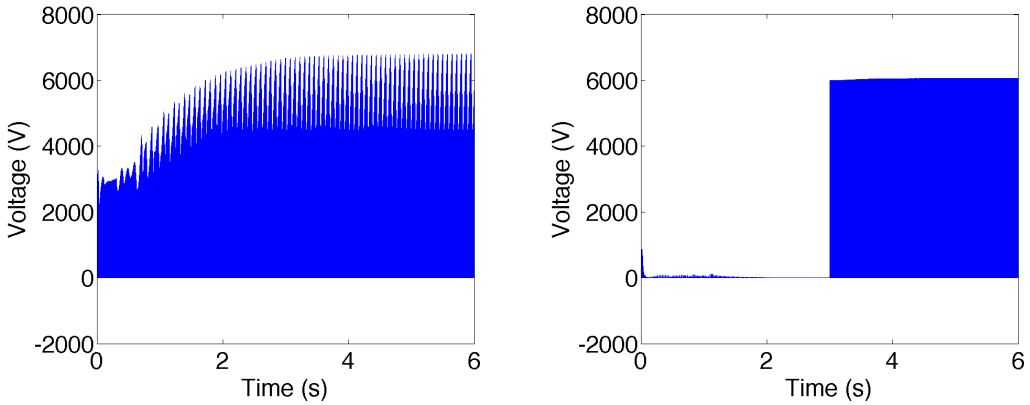

(a) Non-Smooth (b) Smooth

Figure 33. 800VDC Bus Voltage Output, Underway to Hot Standby

well what is occurring, and at 3 seconds the voltage is seen to jump to 6000VDC. This is deceiving due to the solid coloring but, the voltage is actually fluctuating, with a peak value of 6000V (the bus it draws power from), averaging out to 800V, shown in Figure 34.

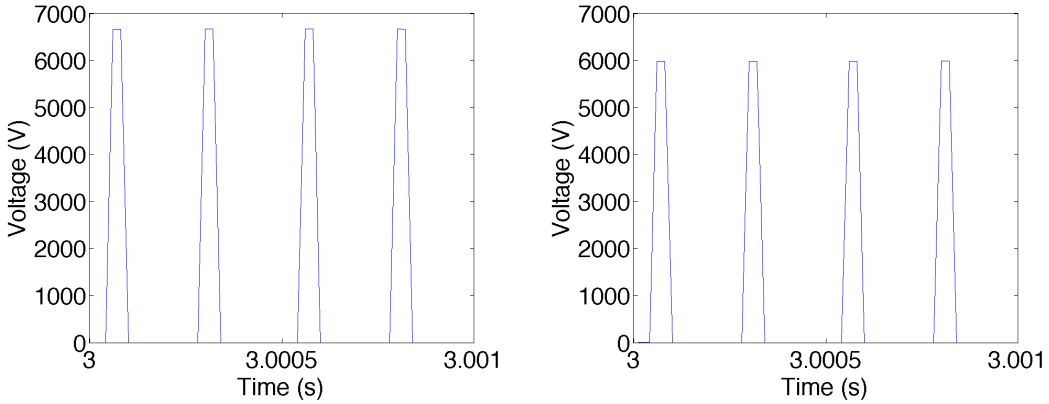

(a) Non-Smooth (b) Smooth

Figure 34. 800VDC Bus Voltage Output-Enlarged, Underway to Hot Standby

4. Hot Standby to Engagement

The third state-of-readiness transition run was from hot standby to engagement. The components that see a change in power draw in this transition are the injector and linac (on the 45kVDC bus), which both go from partial power draw at a 0.5% duty cycle to full power; the beam control is turned from off to on (on the 450VAC bus).

Originally, this run was run for 6 seconds as the others were, with a transition between states of readiness also at 3 seconds. This provided voltage outputs that showed little change from the previous transition. What is important here is the current output because the RF source introduces a very large current load on the 45kVDC bus to fully power the linac and injector at full duty cycle operation. For a relaxation time of just 3 seconds, the steady-state current has not reached a minimum value on the 45kVDC bus. This could be safely ignored for the previous runs since the 45kVDC bus is isolated from the others, and no significant power was demanded from that bus. To solve this, the model was run for a total of 12 seconds, allowing the current to reach a sufficiently low value where the additional current demand from the RF can make an observable difference, and the transition between hot standby and engagement took place at 10 seconds, when the RF is fully powered.

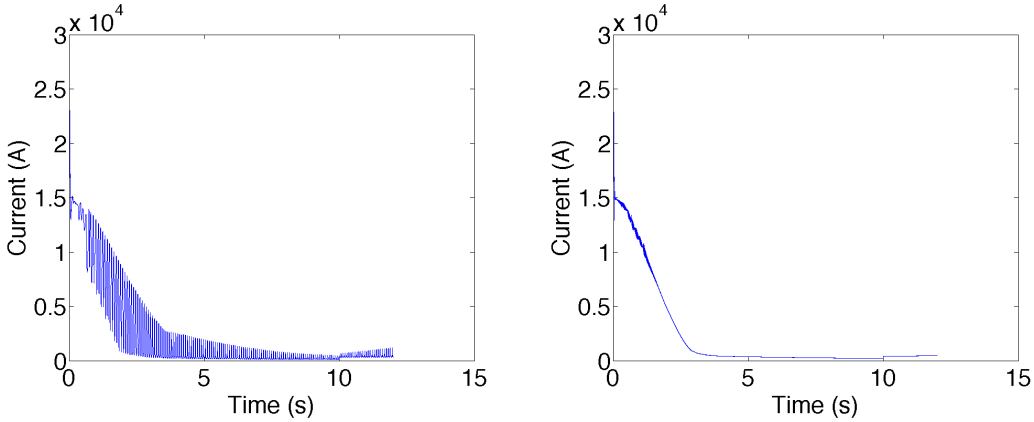

(a) Non-Smooth (b) Smooth

Figure 35. 45kVDC Bus Current Output, Hot Standby to Engagement

Figure 35 shows 45kVDC bus current output for the run in its entirety, for both the smooth and non-smooth models. The current starts out high and quickly approaches its steady-state value. The scale was reduced in Figure 36 to better observe the transition time and the current jump is demonstrated well as the new state demands a higher voltage.

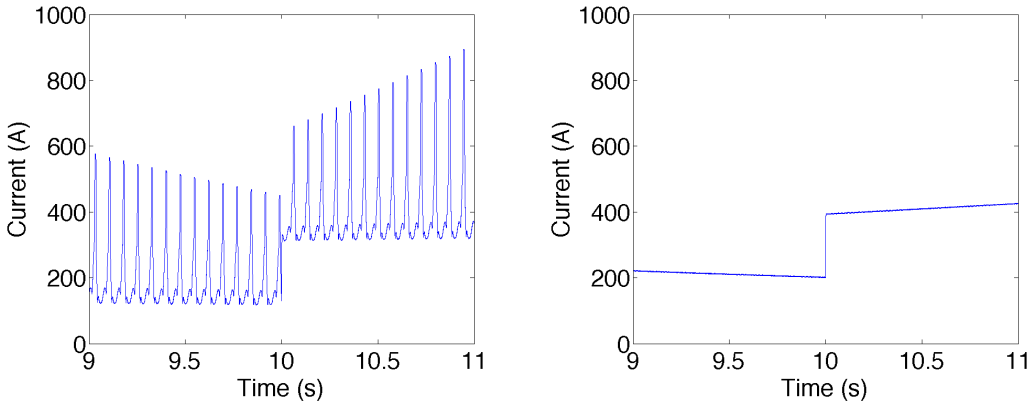

(a) Non-Smooth (b) Smooth

Figure 36. 45kVDC Bus Current Output-Englarged, Hot Standby to Engagement

5. Engagement to Operational Readiness Between Shots

The last state-of-readiness transition modeled was from engagement to operational readiness between shots. The only change in this transition is the turning off of the beam director (on the 450VAC bus). Because this load presents such a small change on the overall system, there were no noticeable changes on the buses, and thus these cases are not shown.

THIS PAGE INTENTIONALLY LEFT BLANK

VI. THE RAILGUN

Artillery has long been a staple of armed warfare, allowing for long-range attacks on an enemy by launching projectiles at their position. This type of weapon has evolved from simple, mechanically driven launchers to advanced barrel-housed projectiles that are fired as exploding gases propel them. Since the First World War, the Navy has invested in this weapon, employed as a deck gun, to fire upon other ships or stage land attacks to clear the way for ground forces. As technology advanced, artillery range and speed began to reach a limit. The maximum muzzle velocity of a fieldable gun, about 1.7km/s, stems from the properties of its propellant gases [17]. Other disadvantages to using explosive-based firing systems are expense and extreme danger. Also, it is difficult to adjust the muzzle velocity of the projectile.

Over the last hundred years, scientists have researched ways to launch projectiles with electricity and magnetism (E&M). Using the idea of a simple, linear motor they developed a way to accelerate a metal projectile via the Lorentz force by completing a circuit across parallel rails. This method is known as the E&M Launcher, or the railgun. In the 1970s, Drs. Richard Marshall and John Barber, of Australian National University in Canberra, developed a railgun powered by 550 Mega-Joules (MJ) of energy stored in capacitor banks that accelerated a 3-gram projectile to 5.9 km/s, reaching what they called hypervelocity [17]. This opened the door to a flood of research and the development of an advanced E&M launcher. Among those searching was the U.S. Navy.

The basic design of a railgun consists of a power source connected to two parallel conductive rails, shown in Figure 37. The source provides a current flow that can be turned off or on with a switch. In between those rails, a sliding armature, which houses the projectile, is placed to complete the circuit. The current flows from the positive terminal of the power source, down the first rail, across the armature and back up the second rail to the negative terminal. This creates a magnetic field around

the rails, which induces a force on the rails and on the sliding armature; namely, the Lorentz force $\boldsymbol{F} = q(\boldsymbol{E} + \boldsymbol{v} \times \boldsymbol{B})$.

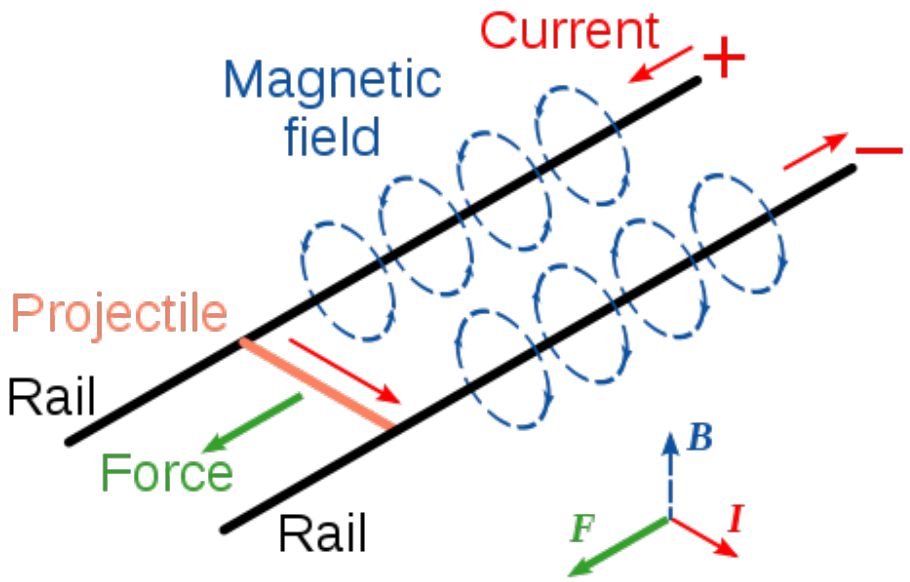

Figure 37. Simple Railgun Design. From [18]

Since the rails are secured they do not move, though it does take a great deal of bracing to secure them. The sliding armature accelerates down the rails, emerging from the railgun at a high velocity.

The work done on the armature in a small displacement of x (dx) is

$$W_{mech} = F \cdot dx. \tag{VI.1}$$

The induced energy in the rails is then calculated as

$$W_{ind} = \frac{dLI^2}{2} = \frac{L'xI^2}{2}, \tag{VI.2}$$

where dL is the change in inductance in the rails, I is the current in rails, $dL = L'dx$, and L' is the inductance gradient per length in the rails. The voltage, V, required

from the power source is

$$V = \frac{L'dxI}{dt} = L'Iv \tag{VI.3}$$

where $v = dx/dt$ is the velocity of the projectile. To calculate the railgun force, conservation of energy is used to find the energy delivered to the circuit

$$W_{delivered} = W_{mech} + W_{ind} \tag{VI.4}$$

$$W_{delivered} = VIdt = L'I^2v\,dt = L'I^2dx \tag{VI.5}$$

$$F = \frac{L'I^2}{2}. \tag{VI.6}$$

Since $W_{mech} = W_{ind}$ the best efficiency achievable is 50%. An important detail for an ideal Naval Shipboard railgun is that the current delivered through the rails to the armature should be as close to constant as possible. This is complicated because the length of the path the current take increases as the armature moves down the rails, so an inductor is used to supply the voltage difference across the rails to provide the constant current needed.

A proposed railgun for the U.S. Navy is estimated to take ∼300MJ from the power source to launch a 20 kilogram (kg) projectile to ∼2.5km/s within a rail-length of 10m. This requires a peak current in the mega-ampere range, and a peak-power in the 10-20 gigawatt range over a millisecond timescale [19]. With these parameters, the railgun is projected to be able to reach ranges of ∼300km and deliver an astounding 17MJ of energy to the target, the equivalent of roughly 4kg of TNT. This proposed gun will later be modeled.

The advantages of the railgun over gas propellant artillery make it an obvious direction for the future of the U.S. Navy. First, the rail gun's range is much greater than conventional artillery, approaching the maximum range of ship-launched or aircraft-launched rockets. This provides a new dynamic of attack, since missiles that cost upwards of five-hundred-thousand dollars per use, such as a BGM-109 Tomahawk missile, can now be replaced with a cheaper and faster alternative.

Propellant-based artillery is costly and volatile, and since railgun projectiles need no chemical propellant, they are cheaper per shot and much safer to store. In addition to lower operational costs and longer ranges than conventional artillery, the railgun also provides tuneability of the muzzle velocity. As previously mentioned, conventional artillery has a mostly fixed muzzle velocity. Since the railgun uses electrical power to propel the projectile, the muzzle velocity can be adjusted to account for target parameters.

VII. THE RAILGUN MODEL

To understand how a system such as the railgun might be incorporated onto the electric ship, modeling of various interactions must be completed. The two procedures that are modeled in this chapter are the charging of a capacitor that will provide energy storage for the railgun, and the firing of a projectile from the railgun. The railgun under consideration has a desired muzzle velocity around 2.5km/s for a 20kg projectile out of a 10 meter (m) long barrel. For this model, the power supply is set to draw power from the 6000VDC bus.

A. POWER SUPPLY AND ENERGY STORAGE

To charge the energy storing capacitor, a system is needed to convert the DC voltage from the ship's 6000VDC bus to 15000VDC. For a 2.0 Farad (F) capacitor, the total stored energy will reach ∼225MJ. To accomplish this, a Buck-Boost DC to DC converter is used. Depicted in Figure 38, a Buck-Boost converter consists of two loops. The left loop consists of a DC voltage source, V_i, a switch, labeled with S, and an inductor, labeled with L. This loop sees current when the switch is closed. The right loop consists of the same inductor, a diode, labeled with D, that prevents

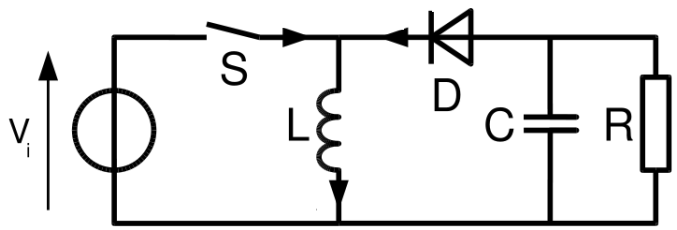

Figure 38. Buck-Boost Converter. From [20]

the capacitor from discharging during the charging cycle, and the capacitor that is

ultimately charged, labeled with C. The current is directed through this loop when the switch is open.

Converting the lower DC voltage to higher voltage is relatively simple. The switch starts out closed, restricting current to the left loop, as seen at the top of Figure 39. When current flows through this loop (red) energy is stored in the inductor. After a short while, the switch is opened so that the current flows through the right loop (red), as seen at the bottom of Figure 39. Now, the energy stored in the magnetic field in the inductor is converted to energy stored in the electric field in the charging capacitor. Before the current stops flowing, the switch flips again and the current through the inductor increases once again, renewing its energy. This process of switching back and forth is repeated until the capacitor reaches its desired charge.

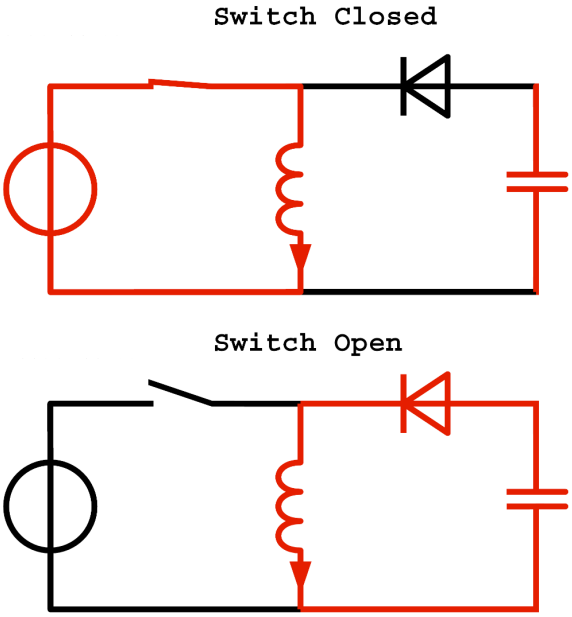

Figure 39. Buck-Boost Converter. Top:Switch Closed. Bottom:Switch Open. After [20]

Components		
Specification	Symbol	Value
Capacitor Charge (Full)	q	30,000C
Capacitance	C	2.0F
Inuctance	L	0.1H
Max Current from power grid	I_{max}	3333.3A
Input Voltage	V_i	6000VDC

Table II. Index of Railgun Component Specifications and Symbols for the Charging Portion

For a nominal electric ship, Table II provides a list of values for each component of this system, and their symbols. These values will later be used when modeling the system. The charge on the capacitor is $q = 30000$C, the capacitance is $C = 2$F the inductance is $L = 0.1$H, the max current is $I_{max} = 3333$A, and the input voltage is $V_i = 6000$VDC

1. The Model

Now that the Buck-Boost converter is understood to be the switching between two circuits, Kirchhoff loops (following Kirchhoff's law $\Sigma V = 0$) must be written for each in order to describe how the system evolves with time. Using these equations, a model has been developed in the C programming language to describe how the charging occurs and in what time frame.

a. Buck-Boost Converter With Switch Closed

When the switch is closed (Figure 40) the current flows from the voltage source and then through the inductor. The Kirchhoff loop for this is then

$$V_i - L\frac{dI}{dt} = 0. \tag{VII.1}$$

Rearranging in terms of $\dot{I}$ yields

$$\frac{dI}{dt} = \dot{I} = \frac{V_i}{L}. \tag{VII.2}$$

If V_i and L are constant, then the solution to the differential equation is

$$I(t) = \frac{V_i}{L}t + I_0, \tag{VII.3}$$

where I_0 is the initial current.

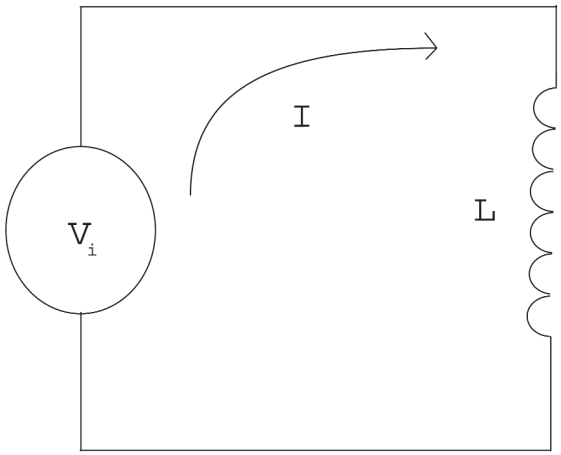

Figure 40. Buck-Boost Converter With Switch Closed

b. Buck-Boost Converter With Switch Open

When the switch is open (Figure 41) the current flows from the inductor to the positive terminal of the capacitor. As mentioned, the direction of the current is constrained by the diode. The Kirchhoff loop for this is

$$L\frac{dI}{dt} + \frac{q}{C} = 0. \tag{VII.4}$$

Solving for $\dot{I}$ gives

$$\ddot{q} = \dot{I} = \frac{-1}{LC}q = -\omega^2 q \tag{VII.5}$$

where $\omega^2 = (LC)^{-1}$.

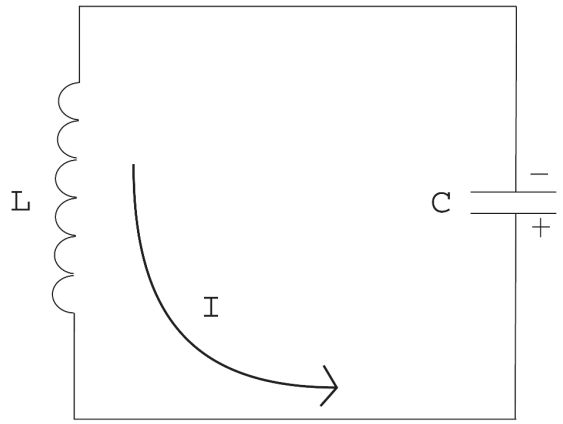

Figure 41. Buck-Boost Converter With Switch Open

If the inductance and capacitance are constant, which they are assumed to be in this model, then the solution to Equation VII.5 is

$$\begin{aligned} q(t) &= q_0 \cos(\omega) + \frac{I_0}{\omega} \sin(\omega t) \\ I(t) = \dot{q}(t) &= -\omega q_0 \sin(\omega t) + I_0 \cos(\omega t). \end{aligned} \tag{VII.6}$$

c. Alternating Between Open and Closed

A realistic power source can only deliver energy at a finite rate. For the present model, the maximum power is set at 20MW, or equivalently, a max current of 3333A. If the switching occurs much more rapidly than the power source can respond, then it is the average current that cannot exceed this value. The average current in this model is defined as

$$\begin{aligned} \langle I \rangle &= \frac{1}{T} \int_0^{t_i} \left[\frac{V_i}{L} t + I_0 \right] dt \\ &= \frac{1}{T} \left[\frac{1}{2} \frac{V_i}{L} t^2 + I_0 t \right] \Big|_0^{t_i} \\ &= \frac{1}{2} \frac{V_i}{L} D t_i + I_0 D \end{aligned} \tag{VII.7}$$

where $D = t_{closed}/T$ and is the fractional duty factor, and t_{closed} =time switch is closed. From this the duty factor can be adjusted dynamically to keep $\langle I \rangle \leq I_{max}$

$$D = \frac{\langle I \rangle}{I_0 + \frac{1}{2}\frac{V_i}{L}t_i}, \tag{VII.8}$$

with the additional constraint $D \leq 1$.

With all of the equations that describe the simulation of charging presented, the charging model can now be run in the C programming language. To do this, a total time-step of $T = 10$ microseconds (μs), and subsequent time-steps when the switch was closed or open of $t_{closed} = T \cdot D$ and $t_{open} = T \cdot (1 - D)$, respectively.

B. RAILS AND PROJECTILE

Now that the charging and energy storage phase is complete, the rails can be used to accelerate a projectile to the desired speed. A simple rail and projectile configuration is pictured in Figure 42. W is the separation between the rails, r is the radius of the rails, x is the distance that the projectile (in red) has traveled down the rails, and I is the current travels through the rails.

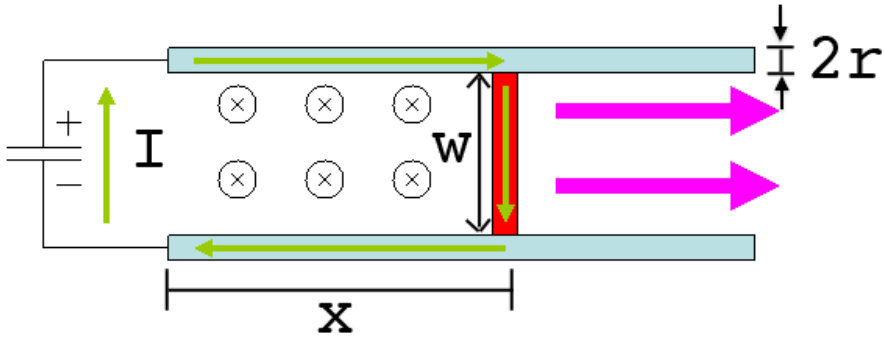

Figure 42. Labeled Rail Dimensions. See Table III for Values. After [21].

Modeling this system can be accomplished using a series of equations developed in this section and depends on several key factors of the rails and the projectile.

Components		
Rail lengths	x	10m
Distance between rails	w	0.15m
Rail radius	r	0.2m
Rail mass	m_r	$\sim$ 10,300kg
Projectile mass	m_p	20kg
Resistivity of Copper Rails	ρ_r	16.8Ω -nm
Mass Density of Copper Rails	ρ_m	$8230kg/m^3$
Specific Heat of Copper Rails	C_h	386 J/kg-K
Temperature Material Constant of Copper Rails	α	4.3mm/m-K
Resistivity of Aluminum Projectile	ρ_p	28.2Ω-nm
Power Supply Resistance	R_c	205$\mu\Omega$
Power Supply Inductance	L_c	5.0μF
Power Supply Capacitance	C	2.0 H

Table III. Index of Railgun Component Specifications and Symbols for the Firing Portion. Ω-ohm, nm-nanometers, mm-millimeters, $\mu\Omega$-micro-Ohm, μF- micro-Farad, H- Henry

Ultimately, what is needed is the force on the projectile at any given time. From this, the acceleration and velocity of the projectile can be determined as it moves down the rails. The necessary values for various components of the Navy's nominal weapons class railgun using copper rails and an aluminum projectile are listed in Table III.

The subsequent sections derive equations describing the solutions of the inductance and resistance in the rails, the resistance in the projectile, the temperature of the rails, the current in the completed circuit, and lastly the force on the projectile.

1. The Model

The Kirchhoff loop for the rail gun current, seen in Figure 43, should include the circuit capacitance (C), circuit resistance (R_c), rail resistance (R), rail inductance (L), and circuit inductance (L_c):

$$\frac{q}{C} - IR_c - IR - \frac{d}{dt}(LI) - L_c\frac{dI}{dt} = 0, \tag{VII.9}$$

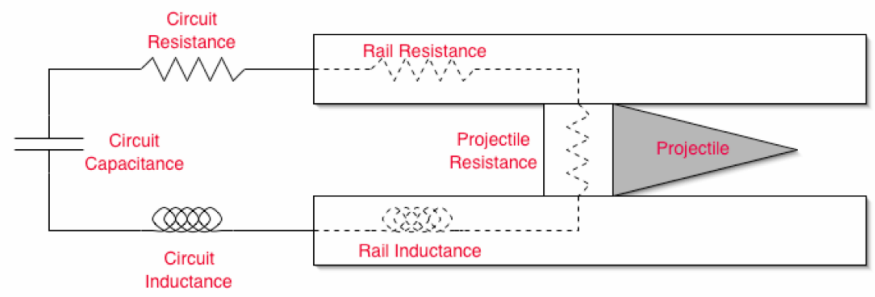

Figure 43. Railgun Circuit-Loop. From [22]

where the total time derivatives of L and I become $d(LI)/dt = L(dI/dt) + I(dL/dt)$, where $dL/dt = L'v$, and v is the velocity of the projectile. For reasons described later, the resistance of the projectile is neglected at this time. The final step is solving for $\dot{I}$, and this is the equation that the C program integrates through to find how the current evolves over time:

$$\frac{dI}{dt} = \frac{q/c - I(R_c + R + L'v)}{L + L_c}. \tag{VII.10}$$

2. Rail Inductance

As current flows through the rails, the resulting inductance L, and magnetic flux, Φ_B, are given by

$$L = \frac{\Phi_B}{I}, \qquad \Phi_B = \int \boldsymbol{B} \cdot d\boldsymbol{A}, \tag{VII.11}$$

where $\boldsymbol{B}$ is the magnetic field induced by the rails, and $\boldsymbol{A}$ is the vector normal to the page with magnitude determined by the rectangular area created from the rails and moving projectile.

Assuming that w is much smaller than the rail length, then the rails can be approximated as infinite wires to determine the resulting magnetic fields. From the Biot-Savart law, the magnetic field at a point s, is given by

$$B(s) = \frac{\mu_0 I}{2\pi}\left(\frac{1}{s} + \frac{1}{2r + w - s}\right).$$

The average value of the field, $\overline{B}$, can be determined via integration

$$\overline{B} = \frac{1}{w}\int_r^{r+w} B(s)\, ds = \frac{\mu_0 I}{\pi w}\ln\left(\frac{r+w}{r}\right). \tag{VII.12}$$

Now using Equation VII.11b the magnetic flux can be determined by

$$\Phi_B = \overline{B} w x = \frac{\mu_0 I x}{\pi}\ln\left(\frac{r+w}{r}\right).$$

Finally, the inductance of the rails at any position of the projectile is written as

$$L(x) = \frac{\Phi_B}{I} = \frac{\mu_0 x}{\pi}\ln\left(\frac{r+w}{r}\right), \tag{VII.13}$$

or as $L(x) = L'x$, where

$$L' = \frac{\mu_0}{pi}\ln\left(\frac{r+w}{r}\right). \tag{VII.14}$$

3. Rail Resistance

The resistance of the rails, R_r, and of the projectile, R_p, would be combined to give total resistance R_{tot}, but since $w \ll$ rail length, R_p is neglected, and R_{tot} is

$$R_{tot} = \frac{2\rho_r x}{\pi r^2},$$

where ρ_r = resistivity of rails.

This estimate can be slightly improved by factoring in temperature dependence. The new temperature-dependent resistance is,

$$R(x, \Delta T) = R_{tot}(1 + \alpha \Delta T), \tag{VII.15}$$

where α is the temperature-material constant of the copper rails, and ΔT is the change in temperature in the rails. The change in temperature is calculated by $\Delta T = \Delta Q/(m_r C_h)$, where C_h is the specific heat, ΔQ is the change in heat given by $\Delta Q = \int_0^t R(x, \Delta T) I^2(t) dt$, and m_r, the rail mass, is given by $m_r = \rho_m(\pi r^2)x$.

4. Force on the Projectile

Now that the material dependent properties of the rails have been developed, and the circuit equations for the current have been described, the force that is experienced by the projectile as it moves down the rails is the last thing to be modeled. The magnetic force on a current carrying object is given by the Lorentz force:

$$F = Iw\overline{B}. \tag{VII.16}$$

Previously, the rails were treated as infinite wires when calculating the magnetic field, but since there is only current running in the loop completed by the projectile, they are now treated as a semi-infinite wire. The magnetic field is then integrated over the distance between the rails to find its averaged value

$$\overline{B} = \frac{1}{w}\int_{r}^{r+w} \frac{\mu_0 I}{2\pi s}\, dS = \frac{\mu_0 I}{2\pi w} \ln\left(\frac{r+w}{r}\right). \tag{VII.17}$$

Putting this into Equation VII.16 now yields the final force equation

$$F = \frac{\mu_0 I^2}{2\pi} \ln\left(\frac{r+w}{r}\right), \tag{VII.18}$$

recalling from Equation VI.6 that $F = L'I^2/2$ and $L' = dL/dx$. The firing simulation will use a time-step of $t = 10\mu s$.

C. RESULTS

The previous sections presented detailed equations that describe the process of charging a capacitor and then using that stored energy to fire a projectile from the railgun. These equations were put into a C-language program where they were evaluated numerically.

1. Charging Results

The charging component was written to simulate five charge and discharge cycles of the capacitor. Figure 44 shows the charge on the capacitor before each shot. After reaching a full charge of 30,000 Coulombs (C), which takes ∼11.2 seconds

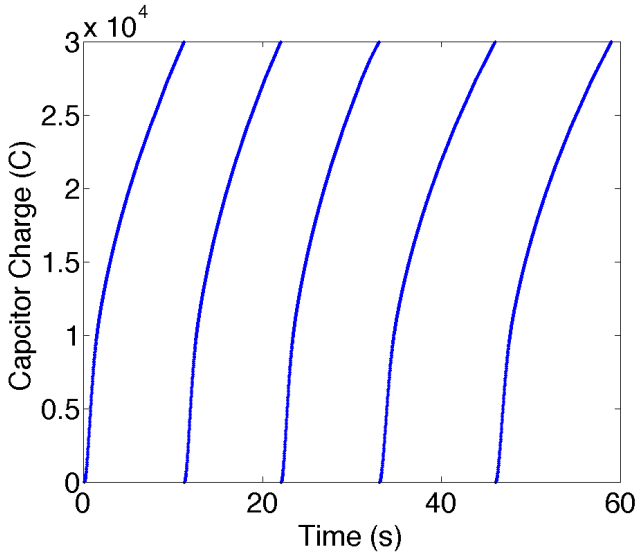

Figure 44. Capacitor Charge, Charging Phase, Five Shots

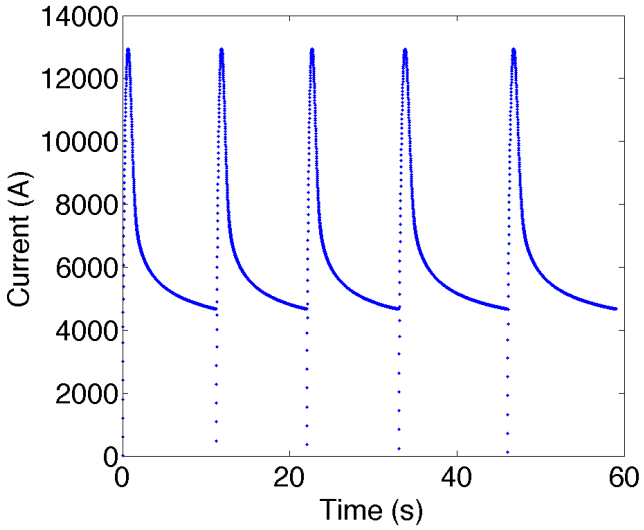

Figure 45. Peak Circuit Current, Charging Phase, Five Shots

for each cycle, the capacitor is depleted by firing a railgun shot. Figure 45 shows the instantaneous current during the charging phase when the switch is closed. It quickly reaches its peak value of about 13kA then quickly drops back to below 5kA as the capacitor slowly reaches its full potential of ∼15kV. With the current at 3333A and the voltage bus supplying 6kVDC, the total power while charging is constant at 20MW, which is the maximum power demand for charging the railgun.

Overall the simulation of the capacitor charging shows that charging a capacitor, or more likely a bank of capacitors, will take on the order of several seconds to reach the full energy (around 230MJ) needed to fire the railgun shots. These results are consistent with what the Navy is expecting to use, about 300MJ as mentioned before. Currently, General Atomics is set to deliver 81MJ capacitor banks to a railgun test facility, and three or four capacitor banks of this type would fulfill the energy requirement of the nominal railgun [23].

2. Firing Results

The firing portion of the model was written to simulate firing one shot. Overall the shot took around 10ms. This is also on the same time-scale that General Atomics expects for its design. The peak velocity of the projectile as it exited the barrel was around 2200m/s, as seen in Figure 46, which is close to the desired specification of 2500m/s [23]. With this muzzle velocity and a mass of 20kg, the projectile leaves the barrel with about 48MJ of energy. This is a decent energy conversion, about 20% efficiency, from the 230MJ stored in the capacitor. The velocity coincides with the acceleration in Figure 47 which shows that the projectile gains most of its velocity in the middle of firing as it reaches about 375km/s^2 (about 38,000 earth gravitational units (Gs)) at 4ms. This acceleration falls under the limits of 40,000Gs that the Naval Surface Warfare Center at Dahlgren predicts.

Figures 48 and 49 show the inductance and resistance as they evolve in the rails. They both increase exponentially, which in turn significantly decreases the voltage across the rails. This is why the projectile gains most of its energy and

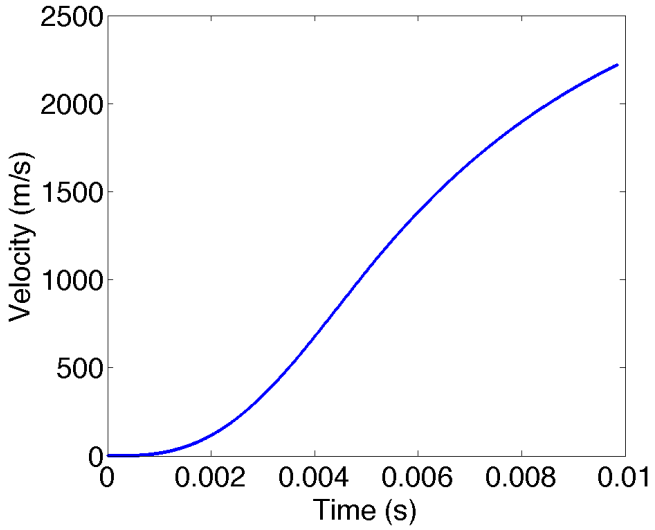

Figure 46. Velocity of Projectile in Barrel During Firing, One Shot

velocity during the first half of the firing.

The capacitors that General Atomics expects to deliver to the Navy as a prototype will deliver about 5.5MA over 10ms to the rails [23]. During firing this simulation reaches a peak current of 8.2MA at about 4.5ms, but averages about 6.0MA over the 10ms time frame for firing. This result is consistent with what General Atomics expects to deliver in capacitor technology, as seen in Figure 50 [23].

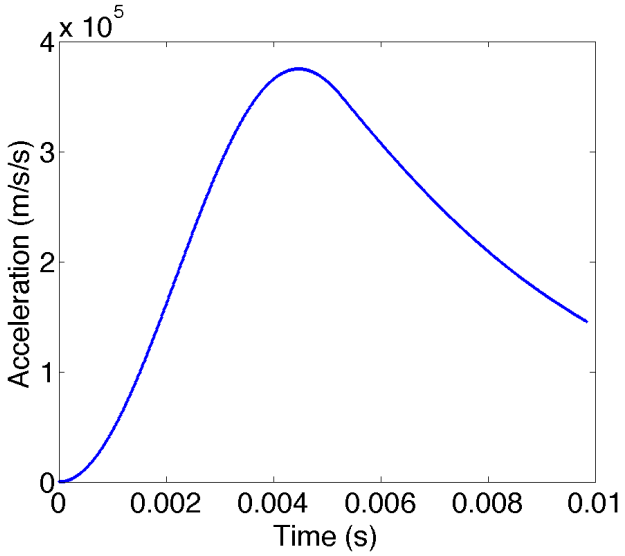

Figure 47. Acceleration of Projectile in Barrel During Firing, One Shot

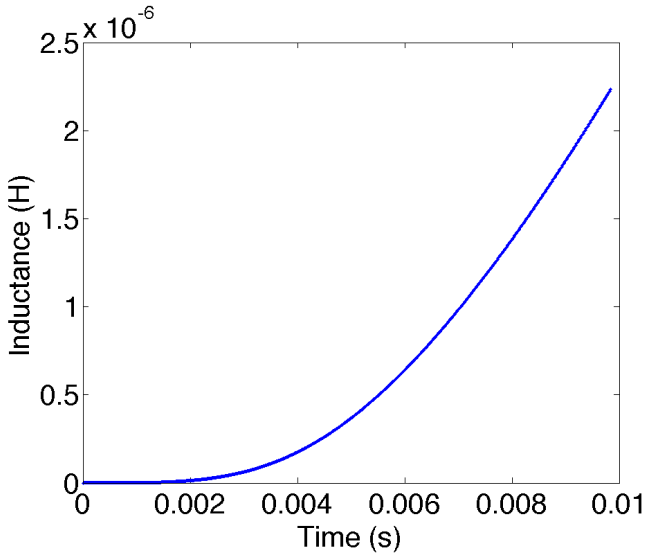

Figure 48. Inductance of Rails During Firing, One Shot

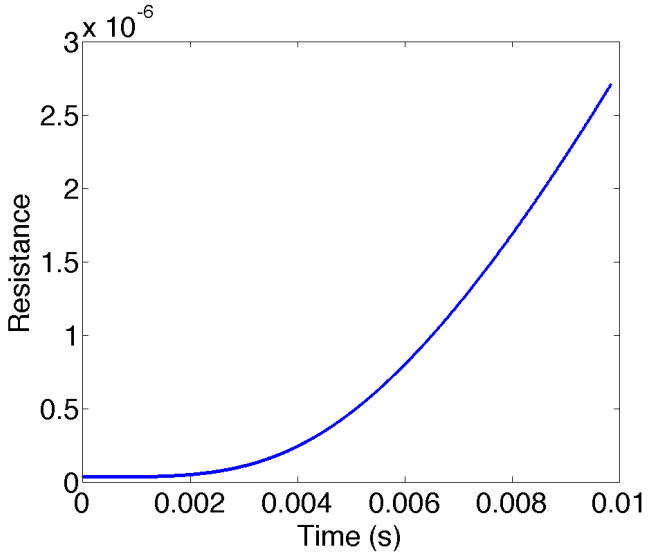

Figure 49. Resistance of Rails During Firing, One Shot

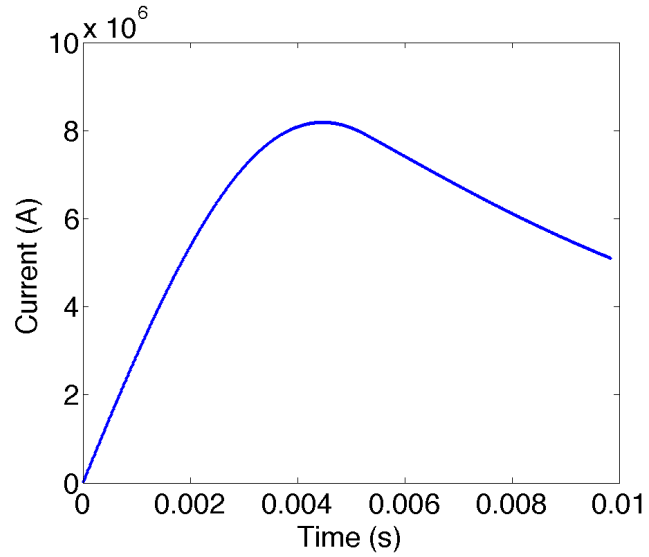

Figure 50. Current in Rails During Firing, One Shot

THIS PAGE INTENTIONALLY LEFT BLANK

VIII. THE LASER WEAPONS SYSTEM

NAVSEA is currently developing a high-powered laser called the Laser Weapons System (LaWS). LaWS is 100kW fiber laser that is designed to be integrated onto the Phalanx Close-In Weapon System (CIWS). The beam director can be retrofitted directly onto CIWS and will use the same targeting system, as seen in Figure 51.

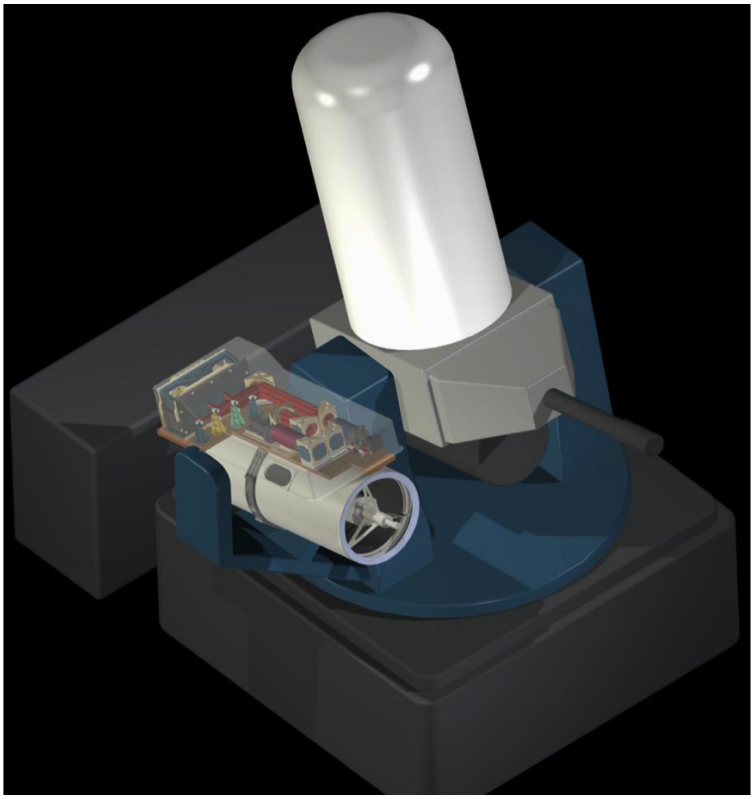

Figure 51. Laser Weapon Systems Integrated Onto Close-In Weapon System. From [24]

To reach laser powers of 100kW, LaWS will combine six Ytterbium fiber lasers into one beam that is directed towards the target. A fiber laser is a type of laser that uses rare-earth elements, such as Ytterbium, as the active gain medium. The gain medium material is stretched into an optical fiber that also serves as the optical

waveguide, providing an easy way to both transport and produce the light. Fiber lasers provide the advantage of good optical quality, high output power, light weight, and reliability [24].

A typical Ytterbium (Yb) fiber laser, such as the YLR and YLS-series developed by IPG Photonics, produces light in the 1070 to 1080nm wavelength region (IPG Photonics). This light typically ranges in power between 10kW and 20kW and is combined with five other beams, as demonstrated in Figure 52, to reach ∼100kW.

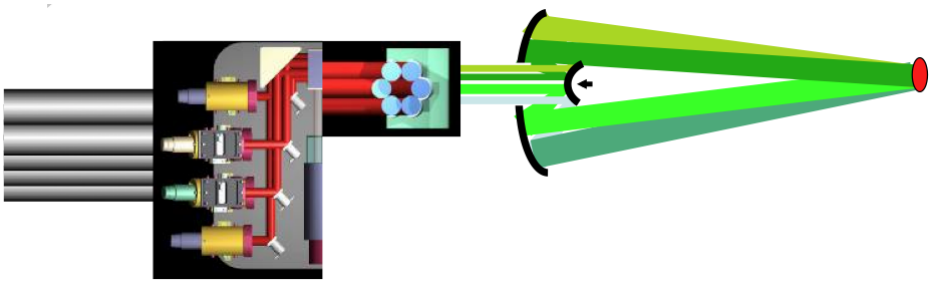

Figure 52. Fiber Optic Laser Merging for Laser Weapons System. From [24]

LaWS needs ∼700kW of average power to operate. The overall wall-plug efficiency for LaWS is ∼14% [24].

After the six beams are merged, they are directed towards the target with a telescopic beam director, 60cm in diameter, mounted on CIWS. Shots last 10 seconds with a 5 second down time in between shots. The telescope also provides a visual surveillance tool for the ship.

It is important to point out that these values are not finalized for what will be aboard a ship, and values are based on NAVSEA estimates from the prototype. The current prototype (Figure 53) has demonstrated lasing, and has successfully shot down UAV's on separate trial runs [24].

In a manner similar to other high power systems, an energy storage device may be needed to reduce the transients on the power grid. While the stored energy might not be used to directly power shots, the energy stored would equalize any

Figure 53. Laser Weapons System Prototype. From [24]

amplitude fluctuations in current or voltage by providing extra power to the ship during heightened demand by all voltage buses [24].

At this time, a model is currently being developed for LaWS, like the FEL and railgun models, but enough information is not yet available to create a relevant model. Over the course of the next few months, further research will take place in collaboration with NAVSEA PMS405.

THIS PAGE INTENTIONALLY LEFT BLANK

IX. CONCLUSION

In conclusion, the most logical choice for the next step in ship power an integrated power system. With that step, electric ships will benefit from a wealth of power available to new systems, such as advanced electric motors, the free electron laser, the railgun, and the laser weapons system.

In summary, this thesis attempted to model the inclusion of high powered systems, specifically the FEL and railgun, on an electric ship. Understanding how these systems integrate onto the electrical grid is key in the development of the systems themselves and of the electric ship.

Through analysis of the FEL model aboard a simulated electric ship power system, much can be learned, as shown in the detailed outputs in this thesis. It is clear that determining the states of readiness and modeling electrical transients when components are turned on are important processes when creating a real world system.

Creating a model for the railgun is important to understanding how the system could be implemented on an electric ship. This thesis showed a method of charging a capacitor and discharging it through the firing of a projectile. All of these values were along the lines of what the U.S. Navy is predicting to use, so the results are very useful for future modeling and understanding.

THIS PAGE INTENTIONALLY LEFT BLANK

LIST OF REFERENCES

[1] B. A. Bassham, "An evaluation of electric motors for ship propulsion," Master's thesis, Naval Postgraduate School, Monterey CA, 2003.

[2] N. H. Doerry, "Next generation integrated power systems for the future fleet," *Corbin A. McNeill Symposium*, 2009.

[3] E. Lundquist, "Navy and industry pursuing new power and propulsion methods," *Weapon Systems Technology Information Analysis Quarterly*, vol. 9, no. 1, pp. 25–30.

[4] O. Bowlin, "Modeling and simulation of the free electron laser and railgun on an electric naval surface platform," Master's thesis, Naval Postgraduate School, Monterey, CA, 2006.

[5] A. Gattozzi (private communication), 2010.

[6] "Solenoid." [Online]. Available: http://en.wikipedia.org/wiki/File:Solenoid.svg. [Accessed: Mar. 26, 2010].

[7] UNSW School of Physics, "Electric motors and generators." [Online]. Available: http://www.animations.physics.unsw.edu.au. [Accessed: Mar. 26, 2010].

[8] D. U. Gubser, "Superconducting coil development and motor demonstration: overview," *Journal of Electronic Materials*, vol. 24, no. 12, pp 1843–1850, 1995.

[9] General Atomics, "Superconducting dc homopolar motor." [Online]. Available: http://atg.ga.com/EM/defense/dc-motor/index.php. [Accessed: Mar. 26, 2010].

[10] American Superconductor, "High temperature superconductor ship propulsion motors." [Online]. Available: http://www.amsc.com/products/motorsgenerators. [Accessed: Mar. 26, 2010].

[11] "Optimal electric ship propulsion solution," *Marine Reporter*, pp. 1–7, 2002.

[12] D. Polka, "What is a drive? electronic motor drives seem to be everywhere, but what are they and how do they work?," ABB Drives and Power Products Group, New Berlin, WI.

[13] Converteam, "Naval electric power, propulsion and control systems." [Online]. Available: http://www.naval-technology.com/contractors/propulsion/converteam/converteam1.html. [Accessed: Mar. 26, 2010].

[14] W. Krupke, "Lasers and sources." [Online]. Available: http://spie.org/x31447.xml?ArticleID=x31447. [Accessed: Mar. 26, 2010].

[15] W. B. Colson, "Free Electron Lasers," Class notes for PH4055, Department of Physics, Naval Postgraduate School, Monterey, CA, SEMESTER 2009.

[16] Defense Daily Industry, "Phalanx ciws: the last defense, on ship and ashore." [Online]. Available: http://www.defenseindustrydaily.com/cat/ordnance-guns/guns-2059-mm-direct. [Accessed: Mar. 26, 2010].

[17] R. A. Marshall and W. Yang, *Railguns: Their Science and Technology*, China Machine Press, 22 Baiwanzhuang Rd. Beijing 100037, China, 2004.

[18] "Railgun." [Online]. Available: http://en.wikipedia.org/wiki/File:Railgun-1.svg. [Accessed: Mar. 26, 2010].

[19] B. Maier, *Selected Topics in Railgun Technology*, Naval Postgraduate School, Spanagel 206A, 2009.

[20] "Buck-boost converter." [Online]. Available: http://en.wikipedia.org/wiki/File:Buckboostconventions.svg. [Accessed: Mar. 26, 2010].

[21] "Physics 210 railgun project." [Online]. Available: http://www.princeton.edu/ romalis/PHYS210/railgun/railgun.html. [Accessed: Mar. 26, 2010].

[22] R. E. Williams, "Naval electric weapons: the electromagnetic railgun and free electron laser," Master's thesis, Naval Postgraduate School, Monterey CA, 2004.

[23] General Atomics, "Advanced weapon launcher systems and technologies." [Online]. Available: http://atg.ga.com/EM/defense/railgun/index.php. [Accessed: Mar. 26, 2010].

[24] NAVSEA (private communication), 2010.

INITIAL DISTRIBUTION LIST

1. Dudley Knox Library
   Naval Postgraduate School
   Monterey, CA
2. Professor Andres Larraza
   Chairman, Physics Department
   Naval Postgraduate School
   Monterey, CA
3. Professor William B. Colson
   Physics Department
   Naval Postgraduate School
   Monterey, CA
4. Professor Keith Cohn
   Physics Department
   Naval Postgraduate School
   Monterey, CA
5. Professor Robert Armstead
   Physics Department
   Naval Postgraduate School
   Monterey, CA
6. Dr. Robert Hebner
   Center for Electromechanics
   University of Texas, at Austin
   Austin, TX